US Army Corps
of Engineers®
Engineer Research and
Development Center

Storm Damage and Flooding Evaluation

Storm-Induced Water Level Prediction Study for the Western Coast of Alaska

Raymond S. Chapman, Sung-Chan Kim, and David J. Mark

October 2009

Storm-Induced Water Level Prediction Study for the Western Coast of Alaska

Raymond S. Chapman, Sung-Chan Kim, and David J. Mark

Coastal and Hydraulics Laboratory
U.S. Army Engineer Research and Development Center
3909 Halls Ferry Road
Vicksburg, MS 39180-6199

Prepared for U.S. Army Engineer District, Alaska

Abstract: The U.S. Army Engineer District, Alaska (CEPOA) has a number of ongoing and potential projects along the western coast of Alaska. At the request of CEPOA, the U.S. Army Engineer Research and Development Center, Coastal and Hydraulics Laboratory (ERDC/CHL) provided technical assistance in assessing storm-generated regional water levels and currents at selected sites. The purpose of this study was to develop frequency-of-occurrence relationships of storm-generated water levels for 17 selected communities along Kotzebue and Norton Sounds, the Bering Sea, and Bristol Bay.

Preface

The U.S. Army Engineer District, Alaska (CEPOA) has a number of ongoing and potential projects located along the western coast of Alaska. At the request of CEPOA, the U.S. Army Engineer Research and Development Center, Coastal and Hydraulics Laboratory (ERDC/CHL) provided technical assistance in assessing storm-generated regional water levels and currents at selected sites. The purpose of this study was to develop frequency-of-occurrence relationships of storm-generated water levels for 17 selected communities along Kotzebue and Norton Sounds, the Bering Sea, and Bristol Bay.

This study was conducted for the CEPOA. Ms. Mary T. Azelton served as the senior coastal engineer; Mr. Kenneth J. Eisses provided direct supervision as well as provided technical support and review for this study. Mr. David Williams served as the study program manager. Research and development activities for this study were conducted at the U.S. Army Engineer Research and Development Center (ERDC), Coastal and Hydraulics Laboratory (CHL), Vicksburg, MS. Drs. Raymond S. Chapman and Sung-Chan Kim, Coastal Processes Branch (HF-C), and Mr. David J. Mark, Estuarine Engineering Branch (HF-EL) performed the study.

This investigation was performed under the direct supervision of Mr. Ty Wamsley, Chief, HF-C, and Dr. Robert McAdory, Chief, HF-E. General supervision was provided by Mr. Bruce A. Ebersole, Chief, Flood and Storm Protection Division. In addition, Dr. William D. Martin served as Director, CHL, and Dr. Rose M. Kress served as acting Deputy Director. COL Gary E. Johnston was Commander and Executive Director of ERDC, and Dr. James R. Houston was Director.

Contents

Unit Conversion Factors

Multiply	By	To Obtain
Feet	0.3048	meters
knots	0.5144444	meters per second
miles (nautical)	1,852	meters
miles (U.S. statute)	1,609.347	meters
miles per hour	0.44704	meters per second
furlongs per fortnight	0.0001663	meters per second

1 Introduction

The U.S. Army Engineer District, Alaska (CEPOA) has a number of ongoing and potential projects located along the western coast of Alaska. At the request of CEPOA, the U.S. Army Engineer Research and Development Center, Coastal and Hydraulics Laboratory (ERDC/CHL) provided technical assistance in assessing storm-generated regional water levels and currents at selected sites. The purpose of this study was to develop frequency-of-occurrence relationships of storm-generated water levels for 17 selected communities adjacent to Kotzebue and Norton Sounds, the Bering Sea, and Bristol Bay (Figure 1-1 and Table 1-1).
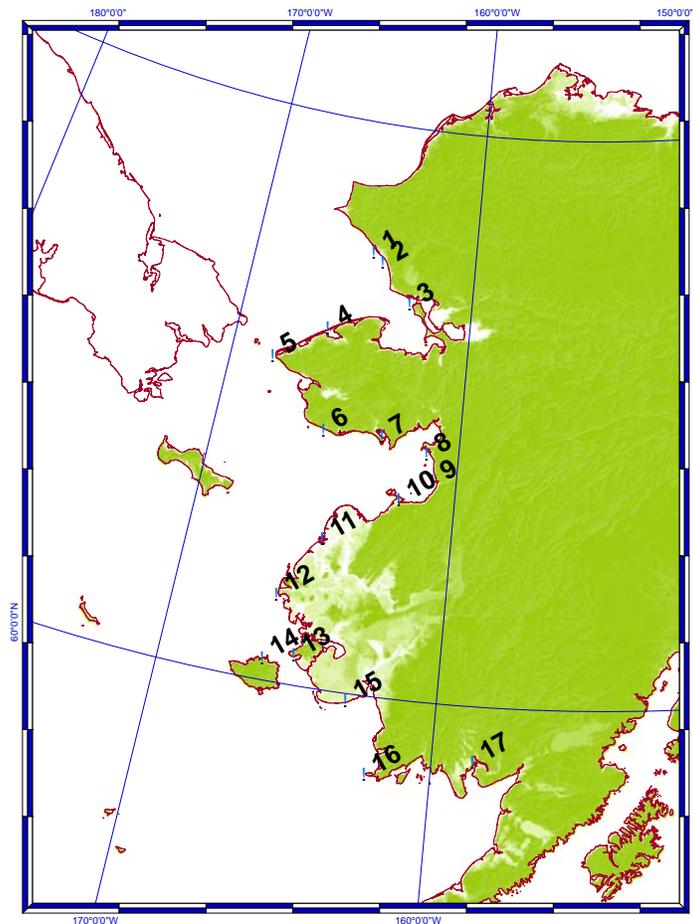
Figure 1-1 Study site

Table 1-1 Site names

Station	Site
1	Kivalina
2	Red Dog
3	Kotzebue
4	Shishmaref
5	Wales
6	Nome
7	Golovin
8	Shatoolik
9	Unalakleet
10	Saint Michael
11	Agcklarok
12	Hooper Bay
13	Toksook Bay
14	Mekoryuk
15	Kongiganak
16	Cape Newenham
17	Dillingham

To accomplish this, a preliminary assessment of Western Alaska storm wind, pressure, ice, and surge data was made. The existing Western Alaska ADCIRC grid (Chapman, et al. 2005) was refined and the bathymetry updated. Calibration and validation simulations were conducted to demonstrate model accuracy. A total of 52 ADCIRC (Appendix B) storm event simulations were performed and a data base of water levels verses return period at each of the 17 sites was developed. A final draft report, "Storm-Induced Water Level Prediction Study for the Western Coast of Alaska" is available that provides the technical methodology, procedures, and discussion.

2 Data Analysis

Wise et al. (1981) discussed parameters that significantly influence coastal storm surge in Alaska. Two major influences are atmospheric and hydrographic effects. Atmospheric parameters include the occurrence of extreme low atmospheric pressure, strong onshore winds, along-shore winds when the shoreline is to the right of the storm track due to the Elman effect, and wind fetch. In addition, the impact of sea ice cover on storm surge was noted. Hydrographic parameters influencing the formation of storm surge are a gently sloping seafloor near shore and sufficient open sea to allow for a long fetch. Wise et al. also developed a subjective forecast procedure for predicting surge height based on fetch (direction and duration), ice cover, lowest pressure, and tidal range at a specific location. In addition, a forecast procedure based on multiple regression analyses for which variables include fetch length, fetch wind, atmospheric pressure, atmospheric stability, and ice cover was presented.

This chapter presents a review and analysis of existing publications, weather event records, tide gage records, and surface meteorological conditions that identify storm surge characteristics of the western Alaska coast. Surface meteorological conditions, which consisted of composite wind, pressure and ice concentration fields provided by Oceanweather (2006), were analyzed. These data consisted of continuous climatology records from 1985 to 2004 and selected hindcast storms that occurred during the 1954-1984 time period (Appendix A).

Records and Publications

Wise et al. (1981) identified 89 historical storm events from 1898 to 1980 in Alaska. The majority of the storms occurred along the western Alaska coast from Kotzebue Sound to Bristol Bay. The most notable event occurred on November 1974 during which nearly the entire western coast of Alaska was affected. Mason et al. (1996) analyzed storm surge events in the Bering Sea from 1898 to 1993 based on newspaper accounts. Among the most notable events, the storms in 1974 and 1992 were identified. Blier et al. (1997) applied the National Weather Service storm surge model for Norton Sound to the October 1992 and August 1993 events. Denise

3

Michels, Mayor, City of Nome, testified before the U.S. Senate Commerce Subcommittee on Disaster Prevention and Prediction for the Western Alaska Winter Storms, in which a chronology of information on the largest storms taken from newspaper articles, publications, the Nome Flood Insurance Study, and other technical documents was presented. Significant storm events noted occurred in 1974, 1992, and 2004. Larsen et al. (http://www.beringseastorm.carolinelarsen.com/) described the October 2004 storm and compared the storm with three other events including the 1974 storm.

The National Oceanic and Atmospheric Administration (NOAA) National Climate Data Center (NCDC) has compiled surge and surf events in Alaska (http://www4.ncdc.noaa.gov/cgi-win/wwcgi.dll?wwevent~storms). Forty-five ocean and lake surf events occurred in Alaska between January 1, 1950 and October 31, 2008; however, none of pre-1993 events were listed. The October 2004 storm was ranked number 31.
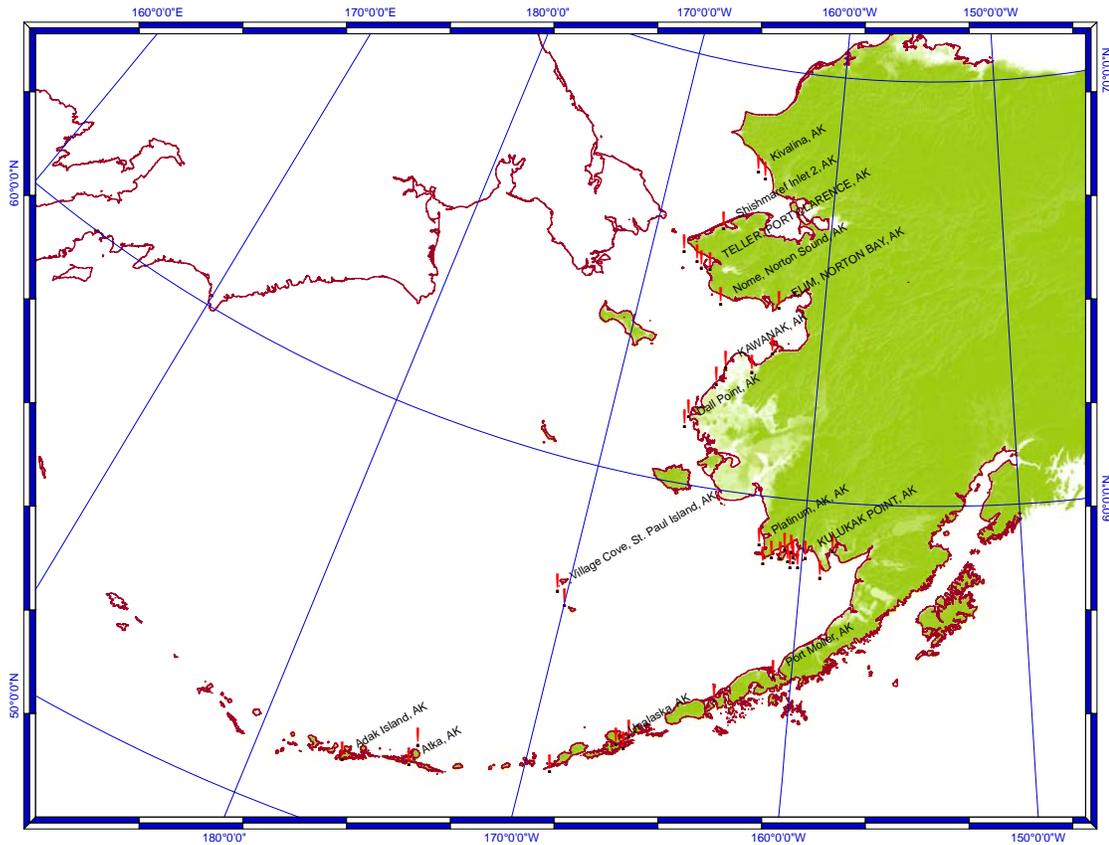
Figure 2-1. Tide gage locations.

The NOAA National Ocean Service (NOS) Center for Operational Oceanographic Products and Services (CO-OPS) maintains tide gage data for a number of sites in western Alaska (http://tidesandcurrents.noaa.gov/index.shtml). Storm surge event water level values were extracted from the gage record archive for these stations (Figure 2-1). Because of the limited record length of the individual gages, there are very few instances where events were recorded at more than one station prior to 2005.

The Nome gage in Norton Sound (NOAA gage 9468756) has the longest record, October 1992 to the present, with a data gap between 1994 and 1997. Figure 2-2 shows the surge events identified as water levels greater than 1 meter above mean seal level (MSL). Two events were identified for the continuous meteorological field period of 1985 to 2004—October 1992 and October 2004. NOS CO-OP lists the 2004 event as the highest water level recorded and the 1992 event as the third highest (Table 2-2). The second highest water level was recorded on September 23, 2005.

The tide gage at Red Dog Dock (NOAA gage 9491094) has been operational since August 2003. NOS CO-OP lists the October 2004 event as the second highest water level recorded. The highest water level was recorded on December 26, 2004, and the third highest water level was record on January 4, 2005. Tables 2-2 and 2-3 list the 10 highest water levels recorded at Nome and Red Dog Dock, respectively. It should be noted that the vertical datum for water levels listed is the local station datum.
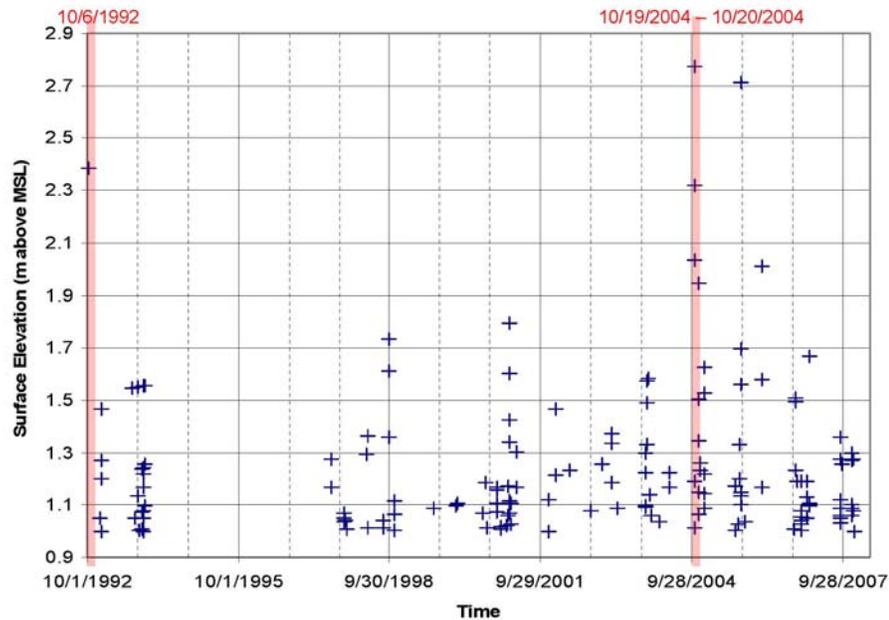
Figure 2-2. Surge events extracted from Nome tide gage.

Table 2-2. Highest extreme water-level events recorded at Nome (source NOAA CO-OP).

Rank	Water level (m)	Time
1	4.12	20041019 17:42
2	4.054	20050923 17:54
3	3.729	19921006 10:54
4	3.665	20041020 05:42
5	3.354	20060215 02:54
6	3.29	20041122 22:48
7	3.14	20010212 03:30
8	3.077	19980924 06:36
9	3.041	20050923 07:12
10	3.014	20070201 01:48

Table 2-3. Highest ten extreme water-level events recoded at Red Dog Dock (source NOAA CO-OP).

Rank	Water level (m)	Time
1	3.697	20041226 09:36
2	3.195	20041020 12:48
3	3.143	20050104 02:42
4	3.068	20080120 23:12
5	3.057	20050104 13:24
6	2.986	20041020 00:42
7	2.977	20050924 07:54
8	2.829	20041021 00:30
9	2.809	20061201 20:24
10	2.779	20060219 13:12

Based on these analyses October 2004 was selected as the model calibration storm event. The October 1992 storm event was selected for model validation.

October 1992 Event

In testimony on March 1, 2006, at U.S. Senate Commerce Sub-committee, Mayor Michels of Nome stated that "a storm in October 1992 severely damaged the revetment on the eastern edge of the seawall." Mason et al. (1996) listed the event as "winds average 29 mph (~ 13 m/s) maximum to 59 mph (~ 26 m/s) from southeast. Winds 58 mph (~ 25 m/s) from southeast, flooding on spit, extensive damage to revetment east of seawall and on Safety spit east of Nome." Blier et al. (1997) provides a detailed analysis of meteorological conditions associated with the October 1992 event and an application of the NWS storm surge model.

Figure 2-3 shows the water surface elevation relative to MSL recorded at Nome. The water level started rising on October 5 and peaked to about 2.5 meters on October 6 around 1200 UTC (Coordinated Universal Time). The water level then rapidly dropped and returned to normal astronomical tide behavior within 2 days. During the event, a low pressure system originated west of the Kamchatka Peninsula and moved rapidly northeastward through the Chukchi Sea. Figure 2-4 shows the time variation of surface pressure and wind speed occurring at a number of locations within and adjacent to Norton Sound. It is seen that the pressure dropped to nearly 960 mb and wind strengthened to more than 18 m/s from the passage of the system, which resulted in the storm surge event.
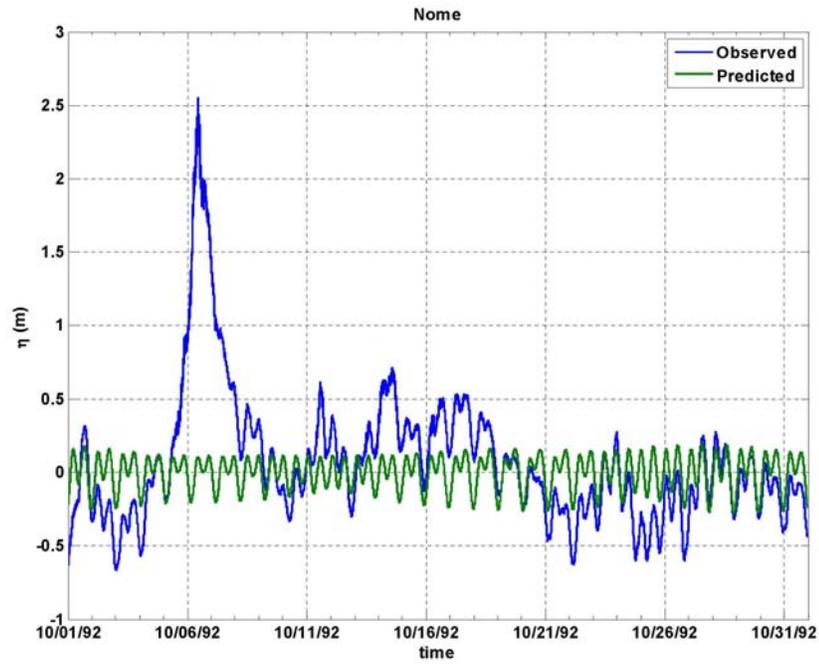
Figure 2-3. Water level record (blue) and predicted tide (green) at Nome during October 1992
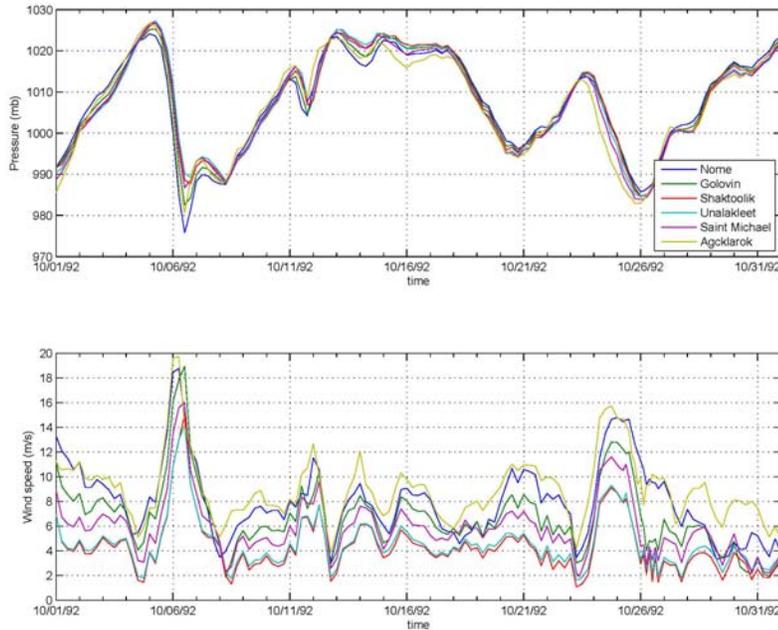
Figure 2-4. Surface pressure and wind speed at selected locations around Norton Sound during October 1992

October 2004 Event

During the Senate testimony, Mayor Michels stated that the "October 19th, 2004 Bering Sea storm caused significant damage and destruction to Western Alaska...recorded an hourly observation during the storm at 55 mph (~ 24 m/s) and a peak tide of 10.5 feet (3.2 meters).The community of Shishmaref lost more land due to erosion. Kotzebue's Front Street was under water....The estimated cost of this disaster is $12,460,469." Larsen et al (http://www.bearingseastorm.carolinelarsen.com/) presents a synoptic overview of the storm.
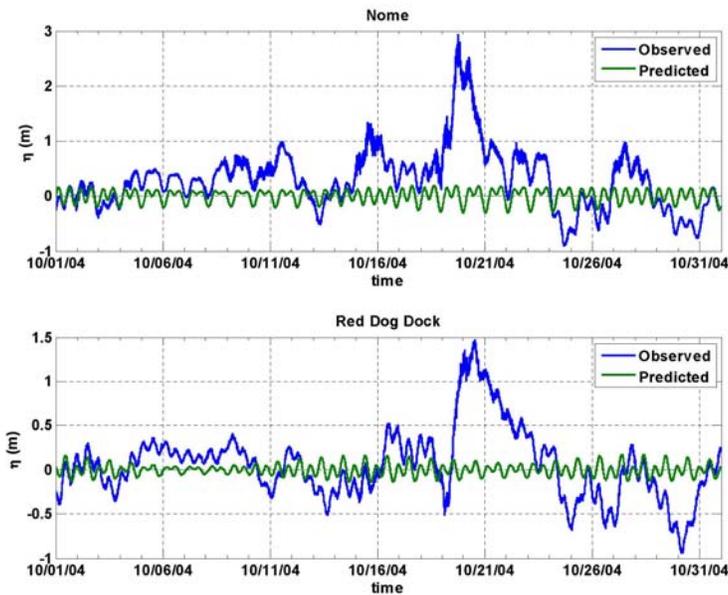
Figure 2-5. Water levels at Nome and Red Dog Dock during October 2004

Figure 2-5 shows the water level at Nome (Norton Sound) and Red Dog Dock (Kotzebue Sound). At Nome, the water level started rising from around October 18, 2004 and peaked on October 19, 2004. It returned to normal within 2 days of the peak. The rise and fall took about 3 days, which is a similar behavior to that of the October 1992 event. At Red Dog Dock, the peak occurred on October 20 and took approximately 3 days to return to normal. Similar to the October 1992 event, the system (central pressure ~ 950 mb) moved northeastward from the east coast of Russia to the Arctic Sea. Figures 2-6 and 2-7 show the surface pressure and wind speed at selected locations in Norton Sound and Kotzebue Sound, respectively. A strong correlation between water levels and meteorological conditions is apparent.
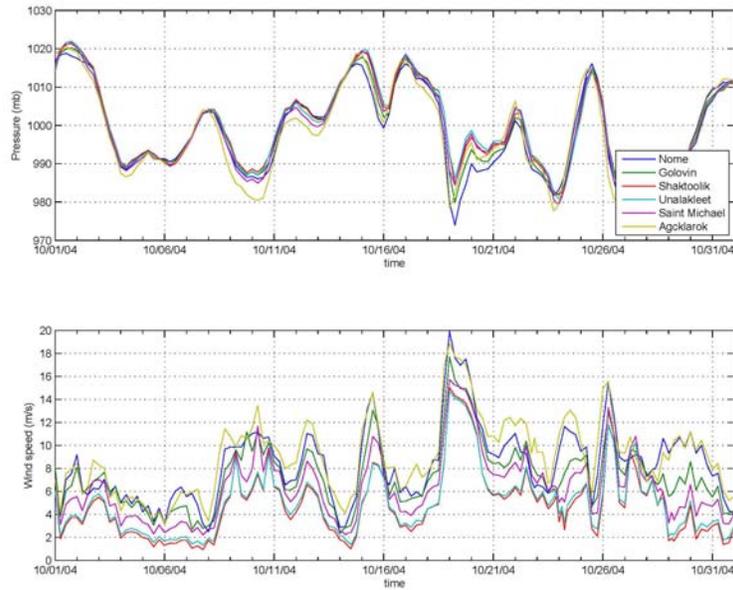
Figure 2-6. Surface pressure and wind speed around Norton Sound during October 2004.
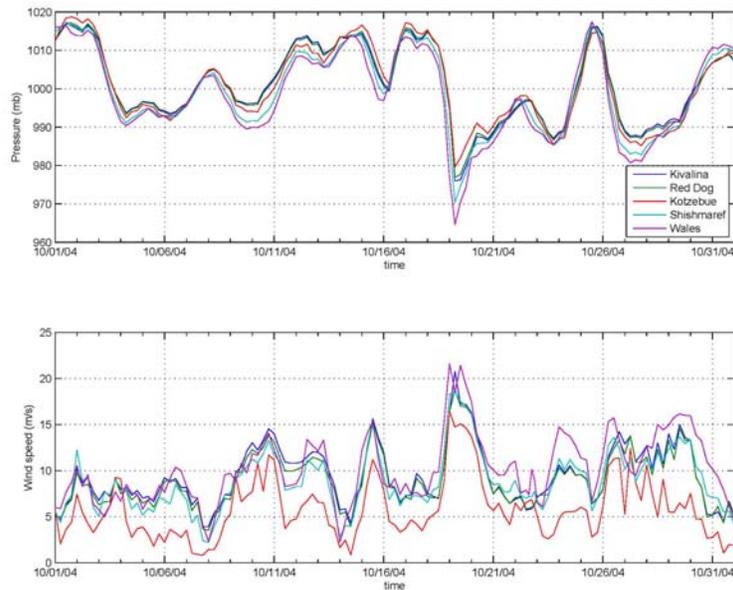
Figure 2-7. Surface pressure and wind speed around Kotzebue Sound during October 2004.

Figures 2-8 and 2-9 show the relationship between water level and surface wind at Nome and Red Dog Dock, respectively. Both show that the

high water levels are associated with the wind from the south and a set-down resulting from a northerly wind.
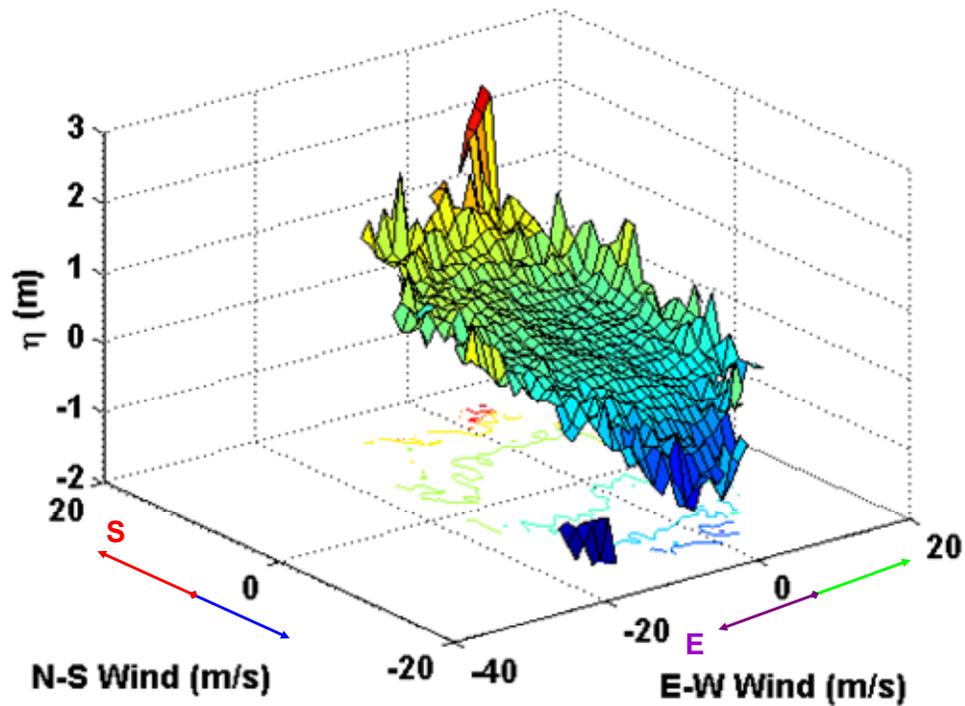
Figure 2-8. Relationship between water level (η) and surface wind at Nome during the tide gage record period of 1992-2004. Red arrow denotes the wind from south and blue arrow denotes the wind from north. Purple and green arrows denote winds from east and west, respectively.
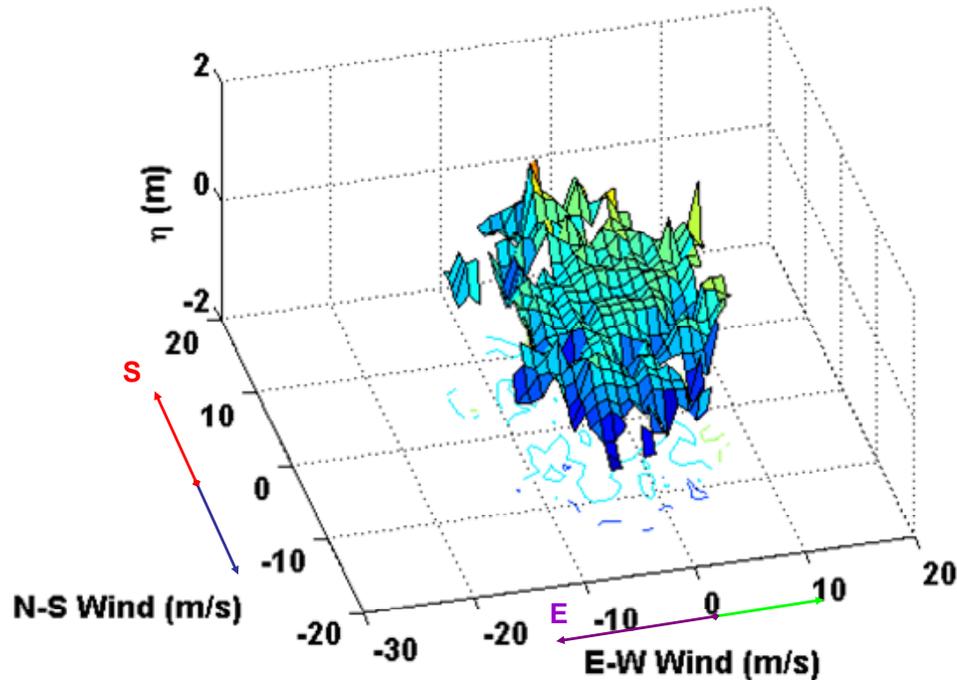
Figure 2-9. Relationship between water level (η) and surface wind at Red Dog Dock during 2001-2004. Red arrow denotes the wind from south and blue arrow denotes the wind from north. Purple and green arrows denote winds from east and west, respectively.

Selection of 1985-2004 Storm Events

To increase the number of storms simulated, an analysis was undertaken to identify appropriated storm events that occurred during the 1985-2004 Oceanweather climatology data gathering. For a typical event such as October 2004, all the coastal locations exhibited similar behavior with differing storm surge magnitudes and phase lags. This suggests that Nome can serve as a reasonable proxy for most meteorological events occurring within the study area.

Based on the analysis above, additional storm events were extracted from the 1985–2004 continuous climatology data when the local winds at Nome exceeded 15 m/s and prevailing direction was from the south. The storm events were defined to have a 7-day duration centered about the peak wind speed. These storm events are listed in Table 2-4.

Selection of 1954-1984 Storm Events

A review of the storm events developed by Oceanweather (Appendix A) revealed that a number of the storms: 1) did not result in a water level setup in the study area; and 2) were of insufficient duration. As a consequence, the far offshore and easterly events were eliminated from the storm population, and the duration of the remaining events was lengthened to 7 days when necessary. The duration of the short-duration storms were lengthened by repeating the first 3-hour wind and pressure field snapshots. The pre-1985 storms are also listed in Table 2-4.

Table 2-4. Simulated storm events.

Year	Month	Year	Month
1954	October	1977	October 10
1955	July	1977	October 18
1957	July	1978	November 2
1960	September	1978	November 8
1960	October	1979	November
1961	June	1982	September
1962	August	1983	October
1962	September	1985	October
1963	August	1985	November
1963	October 1	1988	August
1963	October 6	1989	October
1964	October	1989	November
1965	September	1990	November
1965	November	1991	October
1966	November	1992	October
1968	September	1993	August
1970	November	1993	November
1972	September	1995	October
1972	October	1996	October
1973	July	1996	November
1973	October 1	1998	August

Year	Month	Year	Month
1973	October 15	1998	September
1974	October	2003	November
1974	November	2004	October
1975	August	2004	November
1976	October	2004	December

3 Model Development

Background

This chapter describes the development, calibration, and implementation of the storm surge model for estimating the storm-induced high-water levels used in the frequency-of-occurrence analysis. The ADCIRC (Appendix B) long-wave hydrodynamic model was applied in this analysis. This chapter is composed of four sections, with the first describing the model development, which includes developing the numerical grid. The second section presents the methodology of including the effects of ice in the model. Model calibration is discussed in the third section and model production simulations in the fourth section.

Numerical Grid

The numerical grid used in this study is a modified version of the one developed for the original Western Alaska Storm Surge Study (Chapman, et. al. 2005). Modifications made to the grid include repositioning the grid boundaries for a better agreement with newly released nautical charts, updating grid bathymetry, and increasing resolution in the vicinity of the 17 sites.

The grid boundary along the United States shoreline was aligned with the shorelines extracted from the Electronic Navigational Charts (ENC) database developed by the U.S. National Oceanic and Atmospheric Administration Office of Coast Survey. For areas outside the United States, shoreline positions are aligned with the shorelines extracted from the Digital Nautical Chart (DNC) database published by the U.S. National Geo-spatial Intelligence Agency.

Updated bathymetry incorporated into the present grid was obtained from a number of sources. Bathymetry contained in the DNC were extracted and interpolated onto the grid for areas in international waters and within Russia. Similarly, bathymetry contained in the ENC were extracted and interpolated onto the grid for areas within U.S. coastal waters. However, the ENC did not contain soundings in the region around Hooper Bay and outlying areas. In this region, the bathymetric data were obtained from a database compiled and released by the U.S. Geological Survey,

Alaska Science Center, Walrus Research Program. Additional bathymetry, used in constructing the grid, was obtained from the CEPOA, which included post-dredging surveys. The numerical grid is displayed in Figure 3-1. Figures 3-2 and 3-3 provide examples of grid refinement within Norton Sound.
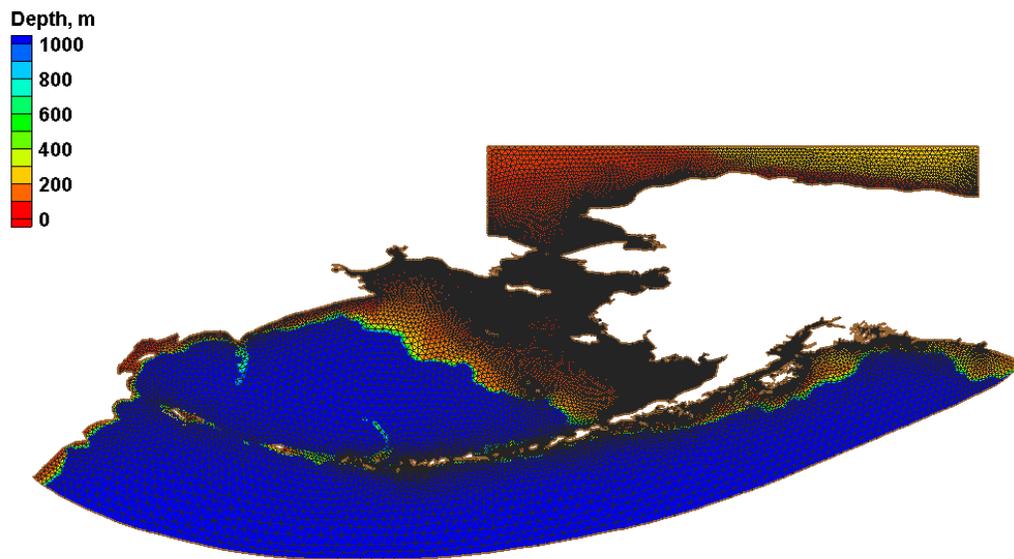
Figure 3-1. Numerical grid (Geographic projection).
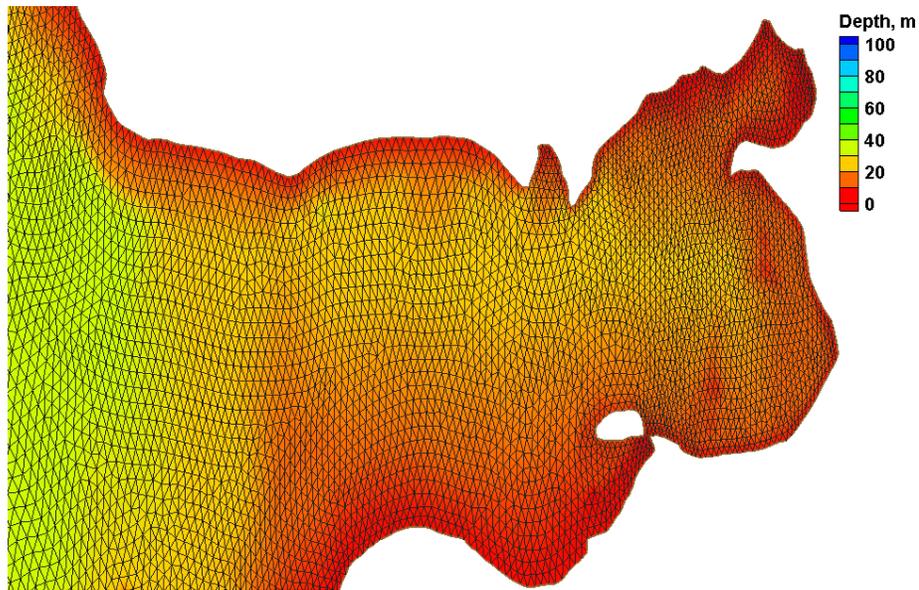
Figure 3-2. Original numerical grid of Norton Sound (UTM projection).
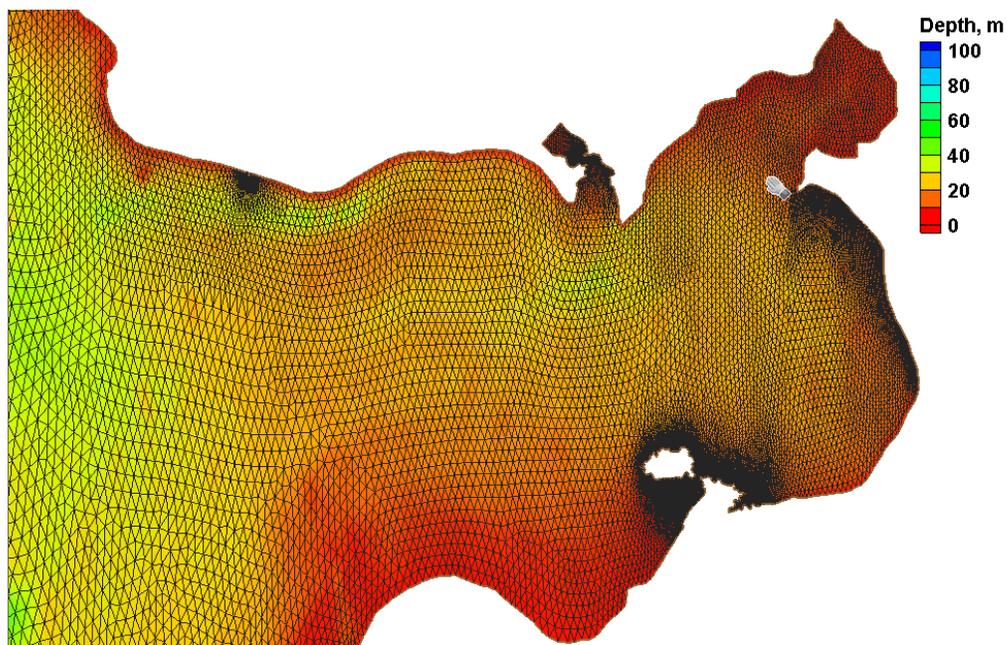
Figure 3-3. Updated numerical grid of Norton Sound (UTM projection).

Ice Concentration Correction

Wind stress drag coefficients traditionally specified in storm surge studies use a wind-wave formulation, such as Garratt (1977), which fit an average empirical equation through a broad range of wind speed measurements. It is generally accepted that for a neutrally stable atmospheric boundary layer, the surface drag coefficient is well estimated by:

$$C_{DN} = (0.75 + 0.067\ U_{10})\ 10^{-3} \qquad (3\text{-}1)$$

where U10 is the 10-meter-height resultant wind speed. However, much research has shown that additional thermal and physical effects need consideration in specifying accurate surface wind stress estimates.

A physical feature influencing surface wind stress in regions such as the Bering, Chukchi and Beaufort Seas is the presence of sea ice as aerodynamic roughness elements. Macklin (1983) and Pease et al. (1983) found that measurements of wind drag coefficients over first year sea ice typically yielded values that were significantly larger and varied less with wind speed than that predicted for open water. More recent work of Birnbaum and Lupkes (2002) and Garbrecht et al. (2002) has formalized the effect of ice form drag on the specification of wind drag coefficients within marginal ice zones. From their work it can be shown that an average empirical fit, to the range of field data, for the air-ice-water wind drag coefficient, C_{DF}, is:

$$C_{DF\ =}\ [0.125 + 0.5\ IC\ (1.0 - IC)]\ 10^{-3} \qquad (3\text{-}2)$$

where IC is the ice concentration varying from 0.0 for open water to 1.0 for complete coverage. Inspection of the air-ice-water wind drag coefficient formula shows that a maximum value of 0.0025 occurs with 50 percent ice coverage. This value is very close to the Macklin (1983) measurement of 0.0028 for first-year ice. Furthermore, the drag coefficient is symmetrical

about 50 percent ice coverage, suggesting that the drag coefficient needed to represent 75 percent ice coverage is close to that of 25 percent ice coverage. This notion is supported by a number of Chukchi and Beaufort Sea storm surge simulations (Henry and Heaps, 1976; Kowalik, 1984; and Schafer, 1966) in which wind drag coefficients greater than or equal to 0.0025 were utilized.   In applying the above air-ice-water surface drag formulation, the value specified according to Equation 3-2 was used to specify a lower limit to the Garratt formula. As an example, the ice-drag coefficient distribution for October 1992 is presented in Figure 3-4.
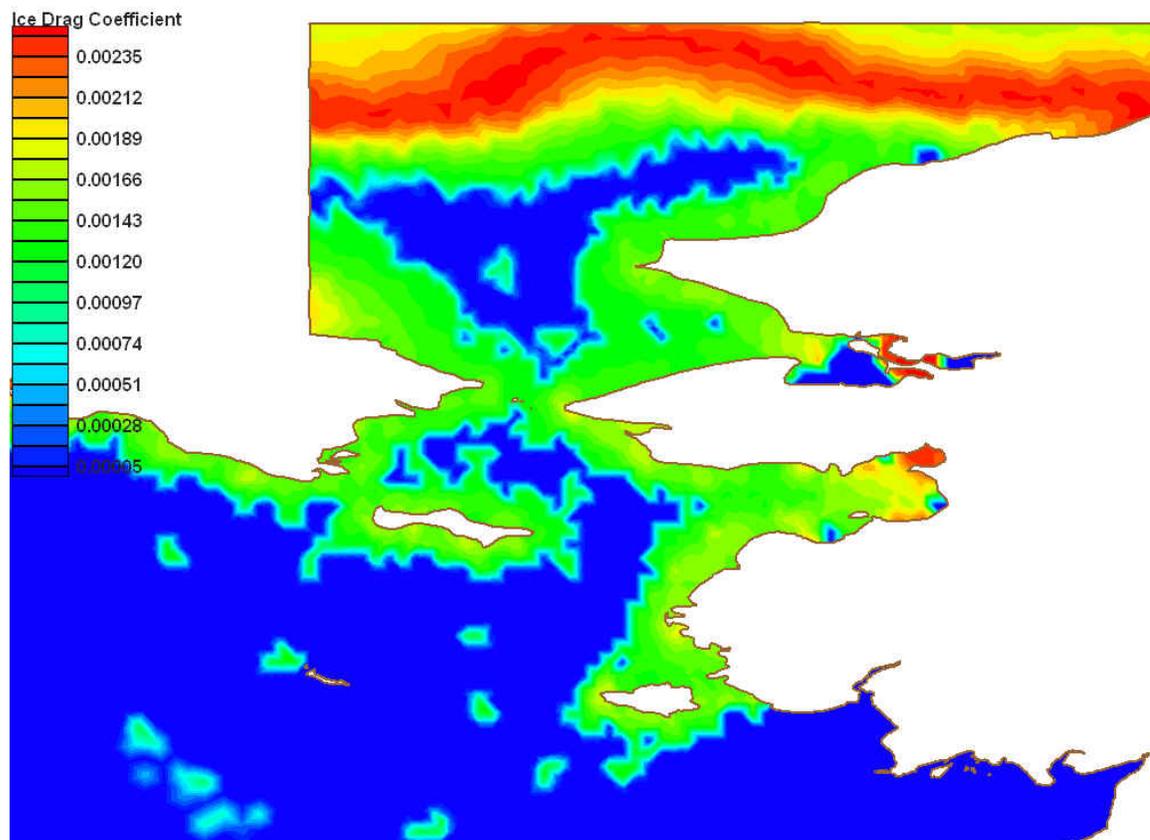
Figure 3-4. Ice-Drag Coefficient Distribution (Geographic projection).

Model Calibration

Calibration and validation of the ADCIRC model was performed using water-surface elevations measured by NOS-maintained gauges at Nome and Red Dog. Satisfactory agreement between predicted and measured water levels during significant wind events provides confidence that the model can accurately replicate storm surges in the study area. As discussed in Chapter 2, the October 2004 storm was selected as the model calibration event and the October 1992 storm as the validation event.

The October 2004 calibration simulation (Figures 3-5 and 3-6) show good agreement between the model-predicted water-surface elevations and observed values at both Nome and Red Dog. The October 1992 predicted and observed water surface elevations at Nome, shown in Figure 3-7, again compare well. Finally, a validation comparison of a weaker storm event that occurred in November 2003 is shown in Figure 3-8. It should be noted that tidal forcing was not included in the model calibration and verification simulations.
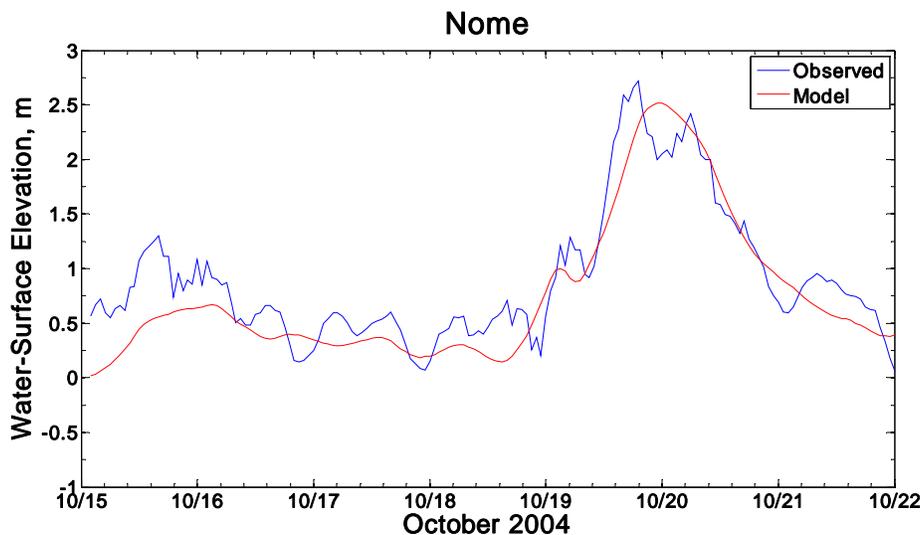
Figure 3-5. Comparison of observed and modeled water levels at Nome, AK; October 2004.
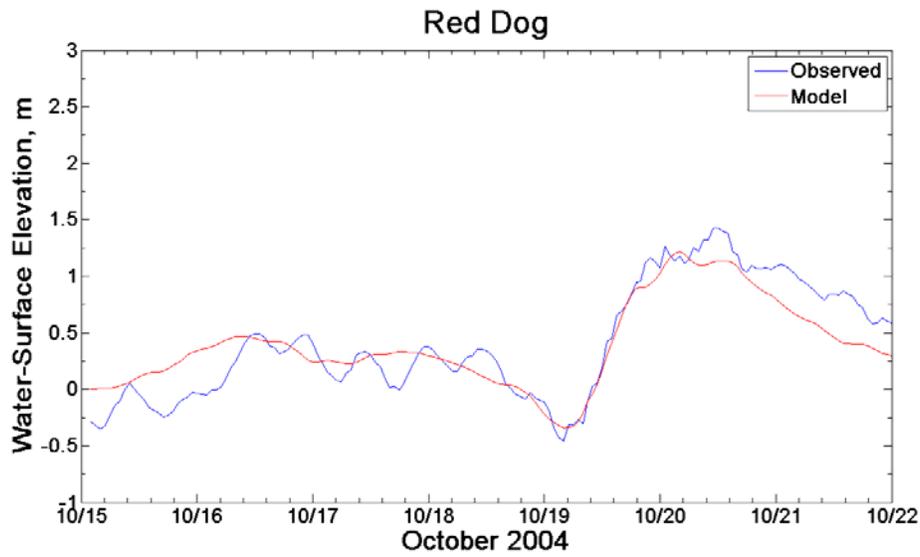
Figure 3-6. Comparison of observed and modeled water levels at Red Dog, AK; October 2004.
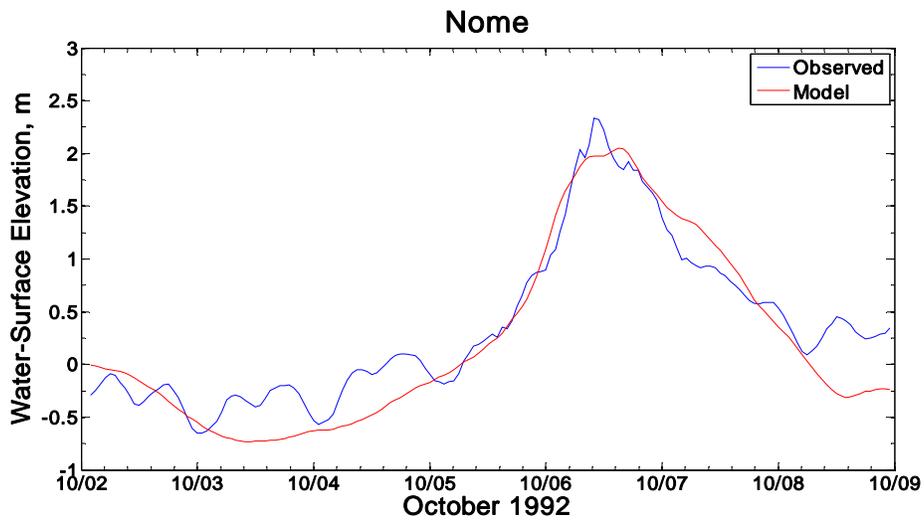
Figure 3-7. Comparison of observed and modeled water levels at Nome, AK; October 1992.
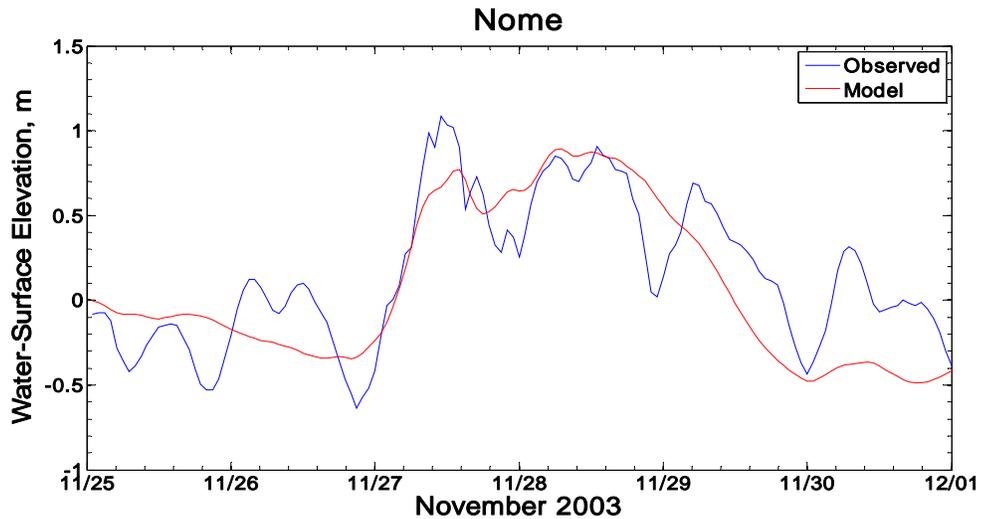
Figure 3-8. Comparison of observed and modeled water levels at Nome, AK; November 2003.

Storm Surge Production Simulations

Subsequent to model calibration and validation, the 52 storm-event production simulations were performed. "One-Line" summaries of the top ten surge elevations, in units of feet mean lower-low water (MLLW), for each site were generated and are presented in Appendix C. An example of the Nome "One Line" summaries, in units of meters mean tide level (mtl), are presented in Table 3-1.

Table 3-1. Nome One-Line summaries

Nome
Location:
  Longitude: 165.4300ºW
  Latitude: 64.5000ºN
Exposure: WSW

Top 10 surge events between 1954 and 2004

	Starting Date	Maximum Water Level (m)	Minimum Surface Pressure	Maximum Wind	
				Speed (m/s)	Direction From
1	10-Nov-74	2.86	969	21.36	S
2	15-Oct-04	2.49	974	19.91	ESE
3	1-Oct-60	2.47	973	21.58	SW
4	8-Nov-78	2.22	994	17.95	S
5	25-Oct-96	2.15	1000	16.21	SSE
6	6-Nov-85	2.02	990	16.67	S
7	14-Nov-66	1.93	994	23.59	SSE
8	1-Oct-55	1.92	969	18.38	SW
9	26-Nov-70	1.89	995	19.32	SE
10	12-Nov-96	1.81	1002	17.08	SSE

4 Storm Event Simulations and Stage-Frequency Analysis

The storms simulated in this analysis are presented in Table 2-4. All storm-surge simulations were performed independently of tidal action, eliminating the task of extracting surge levels from a time-series of combined tide, atmospheric pressure, and surge-induced water-surface elevations.

The Empirical Simulation Technique (EST) was applied to generate stage-frequency relationships (Scheffner and Borgman, 1996). A brief description of EST is presented in Appendix D. Input to the EST model consisted of the predicted peak surge levels. Results of the EST analyses are presented in Tables 4-1 through 4-17, which lists the stage-frequency distribution and standard deviation for return periods ranging between 5 and 100 years at each of the 17 stations.

Table 4-1. Stage-Frequency analysis for Kivalina, AK.

Return Period (years)	Surge Level (m mtl)	Std. Deviation (m)
5	0.98	0.10
10	1.26	0.11
15	1.44	0.17
20	1.59	0.21
25	1.68	0.21
50	1.97	0.27
100	2.23	0.33

Table 4-2. Stage-Frequency analysis for Red Dog, AK.

Return Period (years)	Surge Level (m mtl)	Std. Deviation (m)
5	1.01	0.10
10	1.29	0.11
15	1.48	0.17
20	1.63	0.22
25	1.73	0.22
50	2.01	0.25
100	2.23	0.28

Table 4-3. Stage-Frequency analysis for Kotzebue, AK.

Return Period (years)	Surge Level (m mtl)	Std. Deviation (m)
5	1.12	0.11
10	1.42	0.15
15	1.68	0.22
20	1.85	0.28
25	1.97	0.30
50	2.50	0.56
100	3.10	1.02

Table 4-4. Stage-Frequency analysis for Shishmaref, AK.

Return Period (years)	Surge Level (m mtl)	Std. Deviation (m)
5	0.91	0.12
10	1.18	0.08
15	1.30	0.12
20	1.40	0.14
25	1.47	0.13
50	1.62	0.14
100	1.73	0.12

Table 4-5. Stage-Frequency analysis for Wales, AK.

Return Period (years)	Surge Level (m mtl)	Std. Deviation (m)
5	0.95	0.06
10	1.21	0.11
15	1.32	0.08
20	1.38	0.08
25	1.41	0.08
50	1.53	0.12
100	1.66	0.19

Table 4-6. Stage-Frequency analysis for Nome, AK.

Return Period (years)	Surge Level (m mtl)	Std. Deviation (m)
5	1.53	0.14
10	1.92	0.14
15	2.15	0.18
20	2.31	0.23
25	2.41	0.23
50	2.71	0.30
100	2.97	0.38

Table 4-7. Stage-Frequency analysis for Golovin, AK.

Return Period (years)	Surge Level (m mtl)	Std. Deviation (m)
5	1.83	0.23
10	2.44	0.26
15	2.72	0.21
20	2.86	0.30
25	2.99	0.37
50	3.68	0.82
100	4.46	1.03

Table 4-8. Stage-Frequency analysis for Shaktoolik, AK.

Return Period (years)	Surge Level (m mtl)	Std. Deviation (m)
5	1.76	0.24
10	2.65	0.30
15	3.00	0.28
20	3.23	0.37
25	3.43	0.47
50	4.24	0.89
100	5.12	1.04

Table 4-9. Stage-Frequency analysis for Unalakleet, AK.

Return Period (years)	Surge Level (m mtl)	Std. Deviation (m)
5	1.65	0.24
10	2.58	0.30
15	3.92	0.30
20	3.20	0.40
25	3.39	0.42
50	4.02	0.59
100	4.58	0.65

Table 4-10. Stage-Frequency analysis for St. Michael, AK.

Return Period (years)	Surge Level (m mtl)	Std. Deviation (m)
5	1.53	0.19
10	2.25	0.24
15	2.55	0.26
20	2.78	0.33
25	2.93	0.33
50	3.35	0.38
100	3.69	0.39

Table 4-11. Stage-Frequency analysis for Agcklarok, AK.

Return Period (years)	Surge Level (m mtl)	Std. Deviation (m)
5	1.46	0.15
10	2.05	0.21
15	2.27	0.17
20	2.39	0.21
25	2.52	0.29
50	3.07	0.56
100	3.69	0.68

Table 4-12. Stage-Frequency analysis for Hooper Bay, AK.

Return Period (years)	Surge Level (m mtl)	Std. Deviation (m)
5	1.99	0.15
10	2.47	0.25
15	2.57	0.07
20	2.63	0.10
25	2.69	0.16
50	3.04	0.45
100	3.51	0.66

Table 4-13. Stage-Frequency analysis for Toksook Bay, AK.

Return Period (years)	Surge Level (m mtl)	Std. Deviation (m)
5	1.92	0.16
10	2.45	0.21
15	2.71	0.21
20	2.86	0.25
25	2.98	0.23
50	3.30	0.30
100	3.57	0.36

Table 4-14. Stage-Frequency analysis for Mekoryuk, AK.

Return Period (years)	Surge Level (m mtl)	Std. Deviation (m)
5	1.03	0.07
10	1.30	0.09
15	1.40	0.08
20	1.47	0.12
25	1.55	0.17
50	1.84	0.33
100	2.17	0.41

Table 4-15. Stage-Frequency analysis for Kongiganak, AK.

Return Period (years)	Surge Level (m mtl)	Std. Deviation (m)
5	1.74	0.16
10	2.43	0.32
15	2.84	0.37
20	3.12	0.42
25	3.30	0.39
50	3.79	0.41
100	4.17	0.39

Table 4-16. Stage-Frequency analysis for Cape Dillingham, AK.

Return Period (years)	Surge Level (m mtl)	Std. Deviation (m)
5	1.55	0.14
10	2.13	0.34
15	2.57	0.37
20	2.80	0.39
25	2.97	0.42
50	3.67	0.79
100	4.15	0.98

Table 4-17. Stage-Frequency analysis for Cape Newenham, AK.

Return Period (years)	Surge Level (m mtl)	Std. Deviation (m)
5	0.91	0.07
10	1.16	0.18
15	1.41	0.26
20	1.65	0.38
25	1.82	0.41
50	2.43	0.57
100	2.97	0.62

The EST is based on the assumption that storm-induced water levels consist of identically and independently distributed samples. The extreme value statistics follow the Fisher-Tippet theorem (Fisher and Tippet, 1928). Extreme values are typically represented by one of three statistical distributions, those being the Weibull, Gumbel, or Frechet distribution. The Weibull and Gumbel distributions of the peak storm surge levels were computed for the 17 stations as a "reality check" for the EST results. Compared with the Gumbel approach, the Weibull distribution provided more reasonable estimates for the 10-year and 50-year surge levels. (The 50-year surge level is essentially the same as the greatest peak surge of all the storms simulated, whereas the 10-year surge level is about the same as the peak surge level measured by the NOS gauge, which is 1.91 meters.)

The EST and Weibull distribution provided relatively similar return periods. Furthermore, the stages for the Weibull distributions are generally within one standard deviation of the EST stages for a particular return period. An example comparison of the EST and Weibull estimates for Nome are presented in Tables 4-6 and 4-18.

Table 4-18. Weibull-based Stage-Frequency analysis for Nome, AK.

Return Period (years)	Surge Level (m mtl)
2	1.12
5	1.78
10	2.16
50	2.87
100	3.14

An alternative method of estimating return period is to rank the events over a specific time period (in this study, 51 years between 1954 and 2004) where return period is calculated from

$$T_{return} = \frac{n+1}{m}$$ (4-1)

in which n is the number of years and m is the rank. Fig 4-1 presents a comparison of the EST, Semi-Log, Gumbel and Weibull estimates of frequency-of-occurrence of maximum water levels at Nome over the 51-year analysis period. The EST (red) is bounded by 1 standard deviation. The semi-log fit (green) and estimates using Weibull (blue) distribution and Gumbel (magenta) distribution are bounded by 95 percent confidence interval. The figure suggests that the log-linear fit as well as Weibull and EST yield consistent and reasonable estimates of return period.
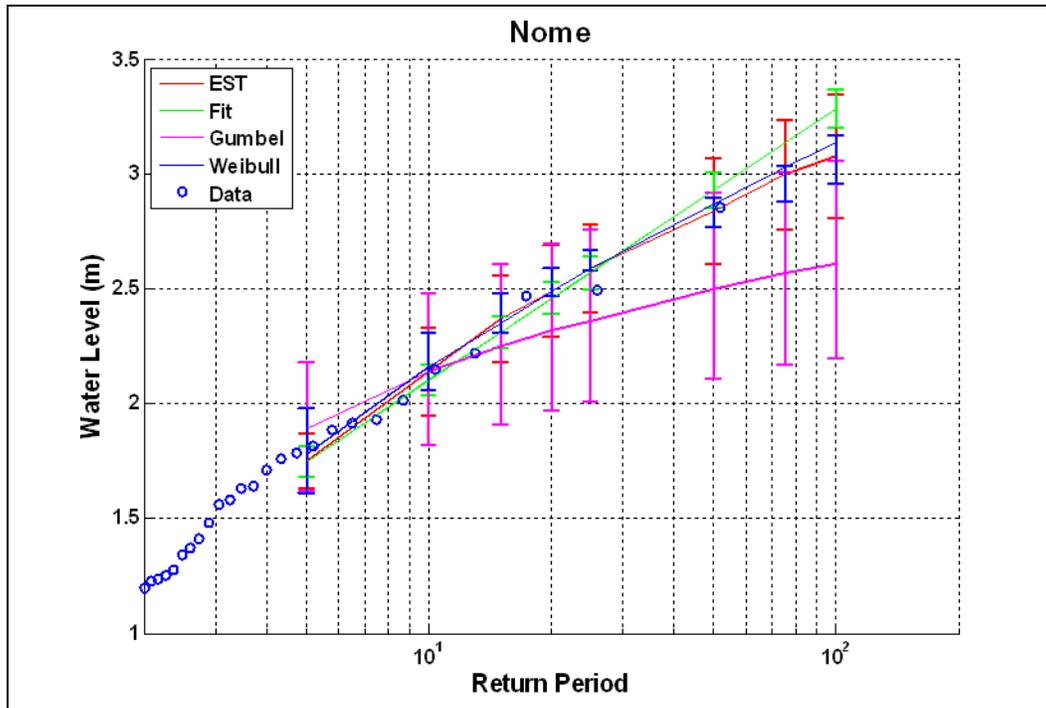
Figure 4-1. Distribution of peak water levels measured at Nome.

A comparison of the EST, Gumbel, Weibull and Semi-Log distribution return periods and water levels (feet MLLW) at all 17 stations is presented in Appendix E. In addition, a comparison plot of the 50-year water level estimates for the 17 stations is presented.

5 Data Archive

The model simulation output data from the 52 storm events was archived for post-processing. These data include water levels and currents for entire model domains as well as input files for ADCIRC runs. Maximum water levels for entire model domains for each storm event are archived separately as a Matlab® binary file. An in-house Matlab data mining utility was developed to use the archived maximum water levels. Given a specified latitude (N) and longitude (W), the program searches for the nearest model node and generates a time series plot of the maximum water levels and estimated return period statistics. An example of a captured screen image is shown in Figure 5-1. A preliminary development effort for presenting data using Google Earth™ has been undertaken. Data presentation in tabular (Figure 5-2) and graphical (Figure 5-3) formats is being developed.
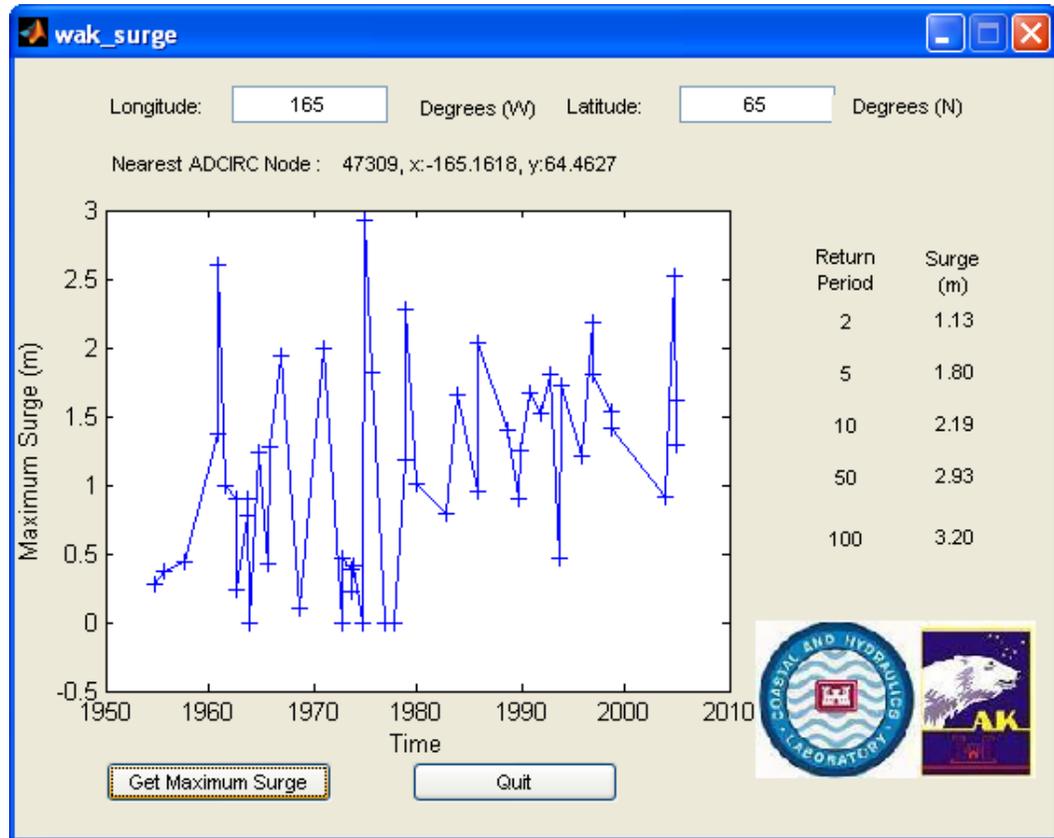
Figure 5-1. Sample output from utility program
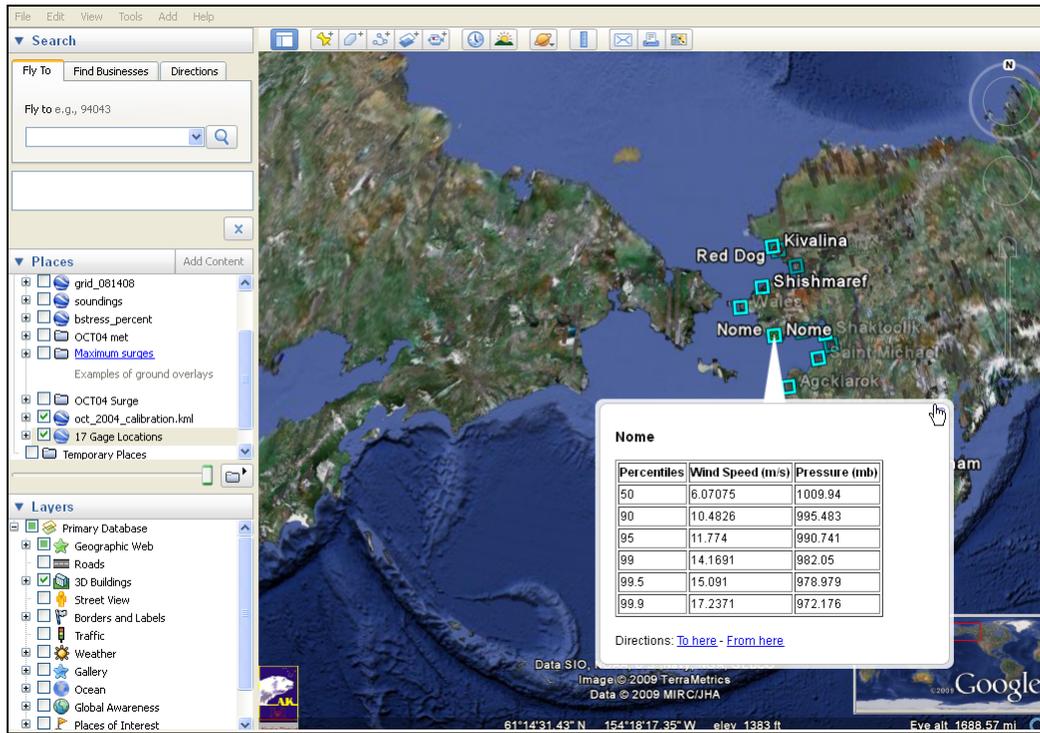
Figure 5-2. Sample output from Google Earth screen shot to show utilizing balloon to disseminate a data in a table form for a location.
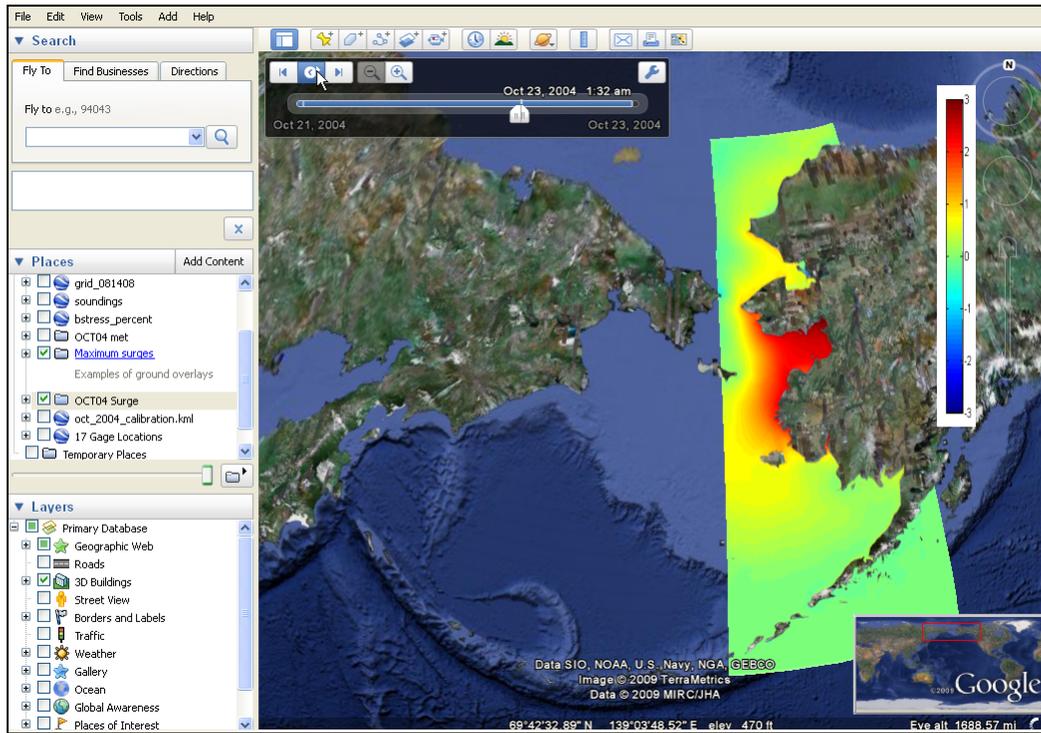
Figure 5-3. Sample output from Google Earth screen shot to show animation of storm surge.

6 Summary

Within the scope of this study, a data analysis has been performed to achieve a greater understanding of the effect of wind forcing, atmospheric pressure, and ice concentration on Western Alaska storm surge water levels. As part of the ADCIRC modeling effort, grid refinements and updated bathymetry were implemented. Calibration and validation simulations were conducted to demonstrate model accuracy. The October 2004 and October 1992 storm surge events were selected for calibration and verification, respectively. A total of 52 storm event simulations were performed, and a data base of corresponding water levels for each of the 17 sites was developed. This data base was subsequently analyzed via an inter-comparison of four statistical techniques to develop the frequency-of-occurrence relationships of storm-generated water levels. The consistency of the frequency-of-occurrence relationships amongst the four statistical methods leads to a reasonable degree of confidence in the return intervals and predicted water levels within and adjacent to Kotzebue Sound and Norton Sound. This results from the fact that adequate model calibration and verification with NOAA gauge data at Red Dog Dock and Nome were available. NOAA gauges installed within and adjacent to Bristol Bay after 2004 can be used to calibrate and verify the model when wind, pressure, and ice field input data from 2005 to the present becomes available. However, until that time, the results for up-estuary sites such as Dillingham and Bethel should be used for reference only. Lastly, data mining tools developed for in-house research have been delivered to the CEPOA.

References

Birnbaum, G. and Lupkes, C. (2002). "A new parameterization of surface drag in the marginal sea ice zone," Tellus, Vol. 74, 107-123.

Blier, W., S. Keefe, W.A. Shaffer, and S.-C. Kim, 1997. Storm surges in the region of the western Alaska. Monthly Weather Review 125, 3094-3108.

Borgman, L., Miller, M., Butler, L., and Reinhard, R. (1992). "Empirical simulation of future hurricane storm histories as a tool in engineering and economic analysis," Proceedings Fifth International Conference on Civil Engineering in the Oceans, ASCE, College Station, TX, 2-5 November 1992.

Borgman, L.E., and Scheffner, N.W. (1991). "Simulation of time sequences of wave height, period, and direction," Technical Report DMP-91-2, U.S. Army Engineer Waterways Experiment Station, Vicksburg, MS.

Chapman, R. S., Mark, D. and A. Cialone (2005). "Regional tide and storm-induced water level prediction study for the West Coast Alaska." Draft Report to POA, U.S. Army Engineer Waterways Experiment Station, Vicksburg, MS.

Fisher. R. A. and L.H. C. Tippett (1928). "On the estimation of the frequency distributions of the largest or smallest member of a sample" Proc. Cambridge Phil. Soc. 24:180–190.

Flather, R.A., (1988). "A numerical model investigation of times and diurnal-period continental shelf waves along Vancouver Island," Journal of Physical Oceanography 18, 115-139.

Garratt, J.R., (1977). "Review of drag coefficients over oceans and continents," Monthly Weather Review 105, 915-929.

Garbrecht, T., Lupkes, C., Hartmann, J. and Wolff, M. (2002), "Atmospheric drag coefficients over sea ice—validation of a parameterization concept," Tellus, Vol. 54 A, pp. 205-219.

Gumbel, E.J. (1954). Statistical theory of extreme values and some practical applications; a series of lectures. U.S. Government Printing Office, Washington, DC.

Henry, R. F. and Heaps, N. S. (1976). "Storm surge in the southern Beaufort Sea," J. Fish. Res. Board Can. Vol. 33, No. 10, pp. 2362-2376.

Kolar, R.L., Gray, W.G., Westerink, J.J., and Leuttich, R.A. (1993). "Shallow water modeling in spherical coordinates: Equation formulation, numerical implementation, and application," Journal of Hydraulic Research.

Kowalik, Z. (1984). " Storm surges is the Beaufort and Chukchi Seas," JGR, Vol. 89, No. C6, pp. 10,570-10578.

Larsen , C, J.E. Walsh, D.E. Atkinson, J. Lingaas, and J. Arnot. A synoptic overview of the severe Bering Sea storm of October 2004 (http://www.bearingseastorm.carolinelarsen.com/)

Luettich, R.A., Jr., Westerink, J.J., and Scheffner, N.W., (1992). "ADCRIC: An Advanced Three-Dimensional Circulation Model for Shelves, Coasts, and Estuaries," Technical Report DRP-92-6, U.S. Army Engineer Waterways Experiment Station, Vicksburg, MS.

Macklin, S. A. (1983) "Wind drag coefficients over first year ice in the Bering Sea. Journal of Geophysical Research. 88, 2845-2852.

Mason, O.K, D.K. Salmon, and S.L Ludwig, 1996. The periodicity of storm surges in the Bering Sea from 1898 to 1993, based on newspaper accounts. Climatic Change 34, 109-123

Pease, C.H., S.A. Macklin, and S.A. Salo (1981): Drag measurements for first-year sea ice ove a shallow sea. Eos, Transactions of the American Geophysical Union 62, 895.

Oceanweather, Inc, (2006) "Wind, pressure and ice concentration fields for Alaska long-term climatology", Contract Report to U.S. Army Engineer Research and Development Center, Vicksburg, MS.

Schafer, P. J. (1966). "Computation of storm surge at Barrow, Alaska," Archiv. Meteorol., Geophys. BioKimatol. Vol. A, No. 15(3-4), pp 372-393.

Scheffner, N.W., and Borgman, L.E., (1993). "Stochastic time-series representation of wave data," Journal of Waterway, Port, Coastal and Ocean Engineering, American Society of Civil Engineers, 118(4), 337-351.

Scheffner, N. W., Clausner, J. E., Militello, A., Borgman, L. E., Edge, B. L., Grace, P. J., (1999). "Use and Application of the Empirical Simulation Technique: User's Guide," Technical Report CHL-99-21, U.S. Army Engineer Research and Development Center, Vicksburg, MS.

Testimony of Denise Michels, Mayor for the City of Nome appearing at the US Senate Commerce Subcommittee on Disaster Prevention and Prediction for the Western Alaska Winter Storms, March 1st, 2006

Wise, J.L., A.L. Comiskey, and R. Becker, Jr., 1981. Storm surge climatology and forecasting in Alaska. Arctic Environmental Information and Data Center, University of Alaska, Anchorage, Alaska

Appendix A: Wind, Pressure, and Ice Concentration Fields for Alaska Long-Term Climatology

Wind, Pressure and Ice Concentration Fields
For Alaska Long-Term Climatology

Work performed under purchase request number WC1JUW-6115-8975

Submitted to:
Robert Jensen
ERDC-Vicksburg

December 25, 2006

Oceanweather
5 River Road
Cos Cob, CT 06807

The goal of this project was to develop a continuous period (1985-2004) and selected storm hindcast (original Shell storms plus 15 new storms, see Table 1) of winds, pressures, and ice concentration data for the Alaska region. Additionally, basin scale winds covering much of the North Pacific were required for each of the time periods for wave model boundary conditions. This work encapsulates several previous projects for Alaska and provides data for all time periods (not just ice free months).

Wind fields within the Region scale (see below) were subject to the Interactive Objective Kinematic Analysis (IOKA) system where individual storms/months were reviewed by an experienced marine meteorologist. Storm periods received additional intensive analysis. Work was performed under purchase request number WC1JUW-6115-8975

Regional Wind Fields

Grid: 50-74N, 155-203E 0.25-degree 3-hourly timestep. Winds on the regional level were tapped from all previous ERDC Alaska projects, plus additional analysis for the Jan-May period not previously reviewed was included. Format: WIN (see below)

Regional Sea Level Pressures

Grid: 50-74N, 155-203E 0.25-degree 3-hourly timestep. Sea level pressures were derived from the NCEP/NCAR reanalysis and spline interpolated onto the target grid. No modifications made. Format: PRE (see below).

Regional Ice Concentrations

Grid: 50-74N, 155-203E 0.25-degree mean monthly. Data sources included gridded ice concentration data from Walsh and Johnson (1953-1978), GSFC (1979-2000) and DMSP (2001-2004). Data were gridded onto the target resolution with sufficient buffer along land boundaries to accommodate an expected regional wave model implementation. Note: data from the Walsh and Johnson period is extremely coarse. All source data obtained from the National Snow and Ice Data Center. Format is a text file that gives the latitude (sLat) and longitude (sLong) and ice concentration (Ice %) in percentage from -1 (no data) to 100 (full ice). The >=050% column give 0=water, 1=ice'd for the 50% threshold.

Basin-Scale Winds

Grid: 10-75N, 110-280E 1.0-degree 6-hourly. Wind fields from the NCEP/NCAR reanalysis were spline-interpolated onto the 1.0 degree grid using the WISPAC QUIKSCAT derived regional corrections. However, unlike the WISPAC Level 2 (NRAQ+) winds, tropical systems were not overlaid. Winds in the domain of the Regional Grid were overlaid onto the basin scale winds for consistency.

Table B1. Storm List.

Reference No.	Starting Date	Ending Date	Source
19541001	1954 10 01 00	1954 10 08 00	Shell
19550717	1955 07 17 06	1955 07 20 06	Shell
19550719	1955 07 19 12	1955 07 22 12	Shell
19551001	1955 10 01 00	1955 10 08 00	OWI
19570715	1957 07 15 00	1957 07 18 00	Shell
19570912	1957 09 12 00	1957 09 15 00	Shell
19600925	1960 09 25 00	1960 09 28 12	Shell
19601001	1960 10 01 00	1960 10 08 00	OWI
19610616	1961 06 16 18	1961 06 19 18	Shell
19620829	1962 08 29 00	1962 09 05 00	OWI
19620903	1962 09 03 12	1962 09 05 18	Shell
19630821	1963 08 21 18	1963 08 24 00	Shell
19631001	1963 10 01 00	1963 10 09 00	Shell
19631006	1963 10 06 00	1963 10 13 00	OWI
19641018	1964 10 18 00	1964 10 21 00	Shell
19641029	1964 10 29 00	1964 11 08 00	OWI
19650905	1965 09 05 00	1965 09 08 00	Shell
19651112	1965 11 12 00	1965 11 19 00	OWI
19661114	1966 11 14 00	1966 11 21 00	OWI
19670915	1967 09 15 00	1967 09 22 00	Shell
19680921	1968 09 21 12	1968 09 23 12	Shell
19701126	1970 11 26 00	1970 12 03 00	OWI
19720928	1972 09 28 00	1972 10 05 00	OWI

19721015	1972 10 15 00	1972 10 18 00	Shell
19730731	1973 07 31 12	1973 08 03 12	Shell
19731001	1973 10 01 00	1973 10 08 00	OWI
19731015	1973 10 15 00	1973 10 17 12	Shell
19741005	1974 10 05 12	1974 10 08 12	Shell
19741022	1974 10 22 12	1974 10 25 12	Shell
19741110	1974 11 10 00	1974 11 18 00	OWI
19750825	1975 08 25 12	1975 08 27 18	Shell
19761025	1976 10 25 00	1976 11 03 00	OWI
19771010	1977 10 10 00	1977 10 13 00	Shell
19771018	1977 10 18 12	1977 10 22 00	Shell
19781007	1978 10 07 00	1978 10 10 00	Shell
19781102	1978 11 02 00	1978 11 07 00	OWI
19781108	1978 11 08 00	1978 11 15 00	OWI
19791003	1979 10 03 12	1979 10 06 12	Shell
19791107	1979 11 07 00	1979 11 14 00	OWI
19791114	1979 11 14 00	1979 11 28 00	OWI
19800926	1980 09 26 12	1980 10 01 00	Shell
19820916	1982 09 16 00	1982 09 24 00	Shell
19831003	1983 10 03 00	1983 10 12 12	Shell
19840928	1984 09 28 00	1984 10 04 00	Shell

```
Oceanweather WIN and PRE File Formats
```

```
Winds and pressure data formats are similar. The header format is the
same,but in the wind file the header is followed by U then V components
whilein the pressure file the header is followed by just pressures.
```

```
The file begins with a header indicating the starting and ending dates and
isfollowed by a grid/date header for each time step and the u and v compo-
nentsof the wind in meters/second or pressures in millibars. Starting/Ending
datesare in YYYYMMDDHH format where:
```

```
YYYY Year
MM Month
DD DayHH
Hour
example win:
```

```
OWI WWS Wind Output Ucomp,Vcomp in m/s Start:1995060600 End:1995060600 iLat=
67iLong= 67DX= 1.250DY= .833SWLat= 22.500SWlon= -82.500Dt=199506060000
```

```
 -1.16856 -1.06439 -.84875 -1.03460 -1.50047 -2.09462 -2.80243 -3.55863 -
 4.24125 -4.84273 -5.59486 -5.37088 -5.30224 -5.12534 -4.89537 -4.67412 -
 4.49203 -4.35772 -4.26612 -4.20260 -4.14746 -4.08396 -4.00686 -3.92213 -
 3.83615 -3.74765 -3.65182 -3.54998 -3.45299 -3.37660 -3.32959 -3.28037 -
 3.10631 -2.67723 -2.08363 -1.53773 -1.12623 -.83526 -.62870 -.47371
```

```
iLat is the number of parallelsiLong is the number of meridionsDX is the grid spacing in
degrees of longitudeDY is the grid spacing in degrees of latitudeSWLat is the latitude of
the South West corner SWlon is the longitude of the South West cornerDt is the date/time in
YYYYMMDDHHmm (same as master header date format but with mm Minutes as well)
```

```
The number of grid points is iLat*iLong, the u component of the winds in meters/second
isfollowed by the v component.
```

```
Sample fortran to read a win file (first time step only):
```

```
 c Read in begining/ending dates of win file10
 format (t56,i10,t71,i10)read (20,10)
 date1,date2
```

```
 c Read Grid Specifications/Date11 format
 (t6,i4,t16,i4,t23,f6.0,t32,f6.0,t44,f8.0,t58,f8.0,t69,i10,i2)read (20,11)
 iLat, iLong, dx, dy, swlat, swlong, lCYMDH, iMin
```

```
 c       Read U/V Components of the
 wind    format (8f10.0)read (20,12)
 ((uu(i,j),i=1,ilong),j=1,ilat)read (20,12)
 ((vv(i,j),i=1,ilong),j=1,ilat)
```

```
Latitude Longitude for each point can be calculated as follows:
```

```
 do 20 icnt = 1,iLatslat(icnt) = SWlat +
 (icnt - 1) * DY20 continue
```

```
 do 30 jcnt = 1,iLongslon(jcnt) = SWlong +
 (jcnt - 1) * DX30 continue
```

```
 Wind Speed/Meteorological Wind Directioncan be com-
 puted from the u/v components as follows:
```

```
        WS = sqrt(uu(iLong,iLat)**2 + vv(iLong,iLat)**2)WDIR =
        mod(180.+atan2d(UU(iLong,iLat),VV(iLong,iLat)),360.)
```

Appendix B: ADCIRC Description

This appendix describes the numerical formulation of the storm surge used in simulating tropical and extra-tropical storms for estimating peak water levels, together with the statistical model used for developing the frequency-of-occurrence relationships based on these peak water levels.

The ADCIRC numerical model was chosen for simulating the long-wave hydrodynamic processes in the study area. When imposing the wind and atmospheric pressure fields, the ADCIRC model can accurately replicate tide induced and storm-surge water levels and currents. The ADCIRC model was developed in the USACE Dredging Research Program (DRP) as a family of two- and three-dimensional finite element-based models (Luettich, Westerink, and Scheffner 1992; Westerink et al. 1992). The model can simulate tidal circulation and storm-surge propagation over very large computational domains while simultaneously providing high resolution in areas of complex shoreline configuration and bathymetry.

In two dimensions, the model is formulated using the depth-averaged shallow water equations for conservation of mass and momentum. Furthermore, the formulation assumes that the water is incompressible, that hydrostatic pressure conditions exist, and that the Boussinesq approximation is valid. Using the standard quadratic parameterization for bottom stress and neglecting baroclinic terms and lateral diffusion/dispersion effects, the following set of conservation equations in primitive, non-conservative form, and expressed in a spherical coordinate system, are incorporated in the model (Flather 1988; Kolar et al. 1993):

$$\frac{\partial U}{\partial t} + \frac{1}{r \cos\phi} U \frac{\partial U}{\partial \lambda} + \frac{1}{R} V \frac{\partial U}{\partial \phi} - \left[\frac{\tan\phi}{R} U + f \right] V =$$

(B-1)

$$- \frac{1}{R \cos\phi} \frac{\partial}{\partial \lambda} \left[\frac{p_s}{\rho_0} + g(\zeta - \eta) \right] + \frac{\tau_{s\lambda}}{\rho_0 H} - \tau_* U$$

$$\frac{\partial V}{\partial t} + \frac{1}{r\cos\phi} U \frac{\partial V}{\partial \lambda} + \frac{1}{R} V \frac{\partial V}{\partial \phi} - \left[\frac{\tan\phi}{R} U + f \right] U =$$

(B-2)

$$- \frac{1}{R} \frac{\partial}{\partial \phi} \left[\frac{p_s}{\rho_0} + g(\zeta - \eta) \right] + \frac{\tau_{s\lambda}}{\rho_0 H} - \tau_* V$$

$$\frac{\partial \zeta}{\partial t} + \frac{1}{R\cos\phi} \left[\frac{\partial UH}{\partial \lambda} + \frac{\partial(UV\cos\phi)}{\partial \phi} \right]$$

(B-3)

where

t = time,

λ and φ = degrees longitude (east of Greenwich is taken positive) and degrees latitude (north of the equator is taken positive),

ζ = free surface elevation relative to the geoid,

U and V = depth-averaged horizontal velocities in the longitudinal and latitudinal directions, respectively,

R = the radius of the earth,

$H = \zeta + h$ = total water column depth,

h = bathymetric depth relative to the geoid,

$f = 2\Omega \sin\varphi$ = Coriolis parameter,

Ω = angular speed of the earth,

p_s = atmospheric pressure at free surface,

g = acceleration due to gravity,

n = Newtonian equilibrium tide-generating potential parameter,

ρ_0 = reference density of water,

$\tau_{s\lambda}$ and $\tau_{s\varphi}$ = applied free surface stresses in the longitudinal and latitudinal directions, respectively, and

τ = bottom shear stress and is given by the expression $C_f(U^2 + V^2)^{1/2}/H$ where C_f is the bottom friction coefficient.

The momentum equations (Equations B-1 and B-2) are differentiated with respect to λ and τ and substituted into the time differentiated conti-

nuity equation (Equation B-3) to develop the following Generalized Wave Continuity Equation (GWCE):

$$\frac{\partial^2 \zeta}{\partial t^2} + \tau_0 \frac{\partial \zeta}{\partial t} - \frac{1}{R\cos\phi}\frac{\partial}{\partial \lambda}\left[\frac{1}{R\cos\phi}\left(\frac{\partial HUU}{\partial \lambda} + \frac{\partial (HUV\cos\phi)}{\partial \phi}\right) - UVH\frac{\tan\phi}{R}\right]$$

$$\left[-2\omega\sin\phi\, HV + \frac{H}{R\cos\phi}\frac{\partial}{\partial \lambda}\left(g(\zeta - \alpha\eta) + \frac{p_5}{l}p_0\right) + \tau_* HU - \tau_0 HU - \tau_{s\lambda}\right]$$

$$-\frac{1}{R}\frac{\partial}{\partial \phi}\left[\frac{1}{R\cos\phi}\left(\frac{\partial HVV}{\partial \lambda} + \frac{\partial HVV\cos\phi}{\partial \phi}\right) + UUH\frac{\tan\phi}{R} + 2\omega\sin\phi\, HU\right] \qquad (B4)$$

$$+\frac{H}{R}\frac{\partial}{\partial \phi}\left(g(\zeta - alfa\eta) + \frac{p_s}{\rho_0}\right) + \tau_* - \tau_0 HV - \frac{\tau_{s\lambda}}{\rho_0}]$$

$$-\frac{\partial}{\partial t}[\frac{VH}{R}\tan\phi] - \tau_0[\frac{VH}{R}\tan\phi] = 0$$

The ADCIRC-2DDI model solves the GWCE in conjunction with the primitive momentum equations given in Equations B-1 and B-2. The GWCE-based solution scheme eliminates several problems associated with finite-element programs that solve the primitive forms of the continuity and momentum equations, including spurious modes of oscillation and artificial damping of the tidal signal. Forcing functions include time-varying water-surface elevations, wind shear stresses, atmospheric pressure gradients, and the Coriolis effect.

The ADCIRC model uses a finite-element algorithm in solving the defined governing equations over complicated bathymetry encompassed by irregular sea/shore boundaries. This algorithm allows for extremely flexible spatial discretizations over the entire computational domain and has demonstrated excellent stability characteristics. The advantage of this flexibility in developing a computational grid is that larger elements can be used in open-ocean regions where less resolution is needed, whereas smaller elements can be applied in the nearshore and estuary areas where finer resolution is required to resolve hydrodynamic details.

Appendix C: One-Line Summaries and EST Frequency-of-Occurrence Tables

Kivalina
Location:
Longitude: 164.5400oW
Latitude: 67.7267oN
Exposure: SW
Top 10 surge events between 1954 and 2004

	Starting Date	Maximum Water Level (ft MLLW)	Minimum Surface Pressure (mb)	Maximum Wind	
				Speed (mph)	Direction
1	10-Nov-74	6.78	965.7	40.5	SSW
2	25-Oct-96	6.75	992.5	43.4	SE
3	26-Nov-70	5.76	978.7	45.4	SW
4	14-Nov-66	5.73	983.5	45.9	SSE
5	08-Nov-78	5.21	992.3	38.9	SSE
6	15-Oct-04	4.62	976.0	46.5	ESE
7	16-Jun-61	4.58	1007.2	32.2	S
8	06-Nov-85	4.55	984.8	42.5	ESE
9	03-Oct-83	4.52	988.4	33.1	NW
10	18-Oct-91	4.32	1001.6	39.1	SW

Frequency of Occurrence

Return Period (years)	5	10	15	20	25	50	100
Surge Level (ft MLLW)	3.67	4.58	5.17	5.67	5.96	6.91	7.77
Std. Deviation (ft)	0.33	0.36	0.56	0.69	0.69	0.89	1.08

Red Dog
Location:
      Longitude: 164.0650°W
      Latitude: 67.5767°N
Exposure: SW

Top 10 surge events between 1954 and 2004

	Starting Date	Maximum Surge (ft MLLW)	Minimum Surface Pressure (mb)	Maximum Wind	
				Speed (mph)	Direction
1	10-Nov-74	6.95	967.1	42.3	S
2	25-Oct-96	6.72	994.1	43.6	SE
3	26-Nov-70	6.32	980.1	45.9	SSW
4	14-Nov-66	5.34	984.4	47.4	SSE
5	08-Nov-78	5.17	992.6	39.4	SSE
6	16-Jun-61	4.72	1008.3	31.3	S
7	03-Oct-83	4.65	988.6	32.9	NW
8	15-Oct-04	4.52	976.9	42.1	ESE
9	06-Nov-85	4.49	985.6	42.3	ESE
10	18-Oct-91	4.39	1001.8	39.1	SW

Frequency of Occurrence

Return Period (years)	5	10	15	20	25	50	100
Surge Level (ft MLLW)	3.76	4.68	5.31	5.80	6.13	7.04	7.77
Std. Deviation (ft)	0.33	0.36	0.56	0.72	0.72	0.82	0.92

Kotzebue
Location:
      Longitude: 162.6000ºW
      Latitude: 66.9000ºN
Exposure: WNW

Top 10 surge events between 1954 and 2004

	Starting Date	Maximum Surge (ft MLLW)	Minimum Surface Pressure (mb)	Maximum Wind	
				Speed (mph)	Direction
1	26-Nov-70	9.18	986.2	47.9	W
2	14-Nov-66	7.12	989.1	49.7	SSE
3	10-Nov-74	6.98	971.7	51.9	S
4	25-Oct-96	6.46	999.3	30.0	SSE
5	29-Aug-62	6.03	989.5	47.0	W
6	03-Oct-83	4.95	989.5	25.7	ESE
7	08-Nov-78	4.85	994.7	46.3	E
8	16-Jun-61	4.75	1011.5	28.9	S
9	01-Oct-60	4.72	966.8	36.0	SSW
10	25-Aug-75	4.69	988.6	28.4	SSW

Frequency of Occurrence

Return Period (years)	5	10	15	20	25	50	100
Surge Level (ft MLLW)	4.06	5.05	5.90	6.46	6.85	8.59	10.56
Std. Deviation (ft)	0.36	0.49	0.72	0.92	0.98	1.84	3.35

Shishmaref
    Longitude: 165.9983°W
    Latitude: 66.2800°N
Exposure: NW

Top 10 surge events between 1954 and 2004

	Starting Date	Maximum Surge (ft MLLW)	Minimum Surface Pressure (mb)	Maximum Wind	
				Speed (mph)	Direction
1	10-Nov-74	6.02	962.4	45.6	SSW
2	26-Nov-70	5.56	984.9	47.6	SSW
3	25-Oct-96	5.53	994.5	42.5	SSE
4	14-Nov-66	4.94	985.7	53.2	SSE
5	08-Nov-78	4.64	990.6	43.2	SSE
6	15-Oct-04	4.55	970.4	41.6	SE
7	01-Oct-60	4.28	965.7	39.1	SSW
8	03-Oct-83	4.28	986.8	33.6	SW
9	18-Oct-91	4.25	1003.9	38.0	SSW
10	06-Nov-85	4.09	986.3	43.4	ESE

Frequency of Occurrence

Return Period (years)	5	10	15	20	25	50	100
Surge Level (ft MLLW)	3.50	4.38	4.78	5.10	5.33	5.82	6.19
Std. Deviation (ft)	0.39	0.26	0.39	0.46	0.43	0.46	0.39

Wales
Location:
   Longitude: 168.0900°W
   Latitude: 65.6100°N
Exposure: SW

Top 10 surge events between 1954 and 2004

	Starting Date	Maximum Surge (ft MLLW)	Minimum Surface Pressure (mb)	Maximum Wind	
				Speed (mph)	Direction
1	10-Nov-74	5.37	957.7	54.1	S
2	12-Nov-96	5.33	998.1	46.5	SE
3	06-Nov-85	5.00	984.1	38.7	E
4	15-Oct-04	4.97	964.6	48.3	E
5	25-Oct-96	4.87	991.6	47.2	SSW
6	08-Nov-78	4.71	988.0	55.3	SSE
7	16-Nov-90	4.58	986.3	40.3	E
8	14-Nov-66	4.41	985.1	56.6	SSE
9	02-Oct-92	4.28	969.4	41.4	SE
10	19-Nov-04	3.82	979.2	37.6	E

Frequency of Occurrence

Return Period (years)	5	10	15	20	25	50	100
Surge Level (ft MLLW)	3.63	4.48	4.84	5.04	5.14	5.53	5.96
Std. Deviation (ft)	0.20	0.36	0.26	0.26	0.26	0.39	0.62

Nome
Location:
     Longitude: 165.4300ºW
     Latitude: 64.5000ºN
Exposure: SSW

Top 10 surge events between 1954 and 2004

	Starting Date	Maximum Surge (ft MLLW)	Minimum Surface Pressure (mb)	Maximum Wind	
				Speed (mph)	Direction
1	10-Nov-74	10.12	968.5	47.9	S
2	15-Oct-04	8.94	974.0	44.5	ESE
3	01-Oct-60	8.87	973.2	48.3	SW
4	08-Nov-78	8.05	993.6	40.3	SSE
5	25-Oct-96	7.82	1000.2	36.2	S
6	06-Nov-85	7.40	990.1	37.4	SSE
7	14-Nov-66	7.07	993.8	52.8	SSE
8	26-Nov-70	6.97	994.5	43.2	SW
9	12-Nov-96	6.71	1002.4	38.3	SE
10	02-Oct-92	6.64	975.8	42.1	SSE

Frequency of Occurrence

Return Period (years)	5	10	15	20	25	50	100
Surge Level (ft MLLW)	5.79	7.07	7.82	8.35	8.68	9.66	10.51
Std. Deviation (ft)	0.46	0.46	0.59	0.75	0.75	0.98	1.25

Golovin
Location:
 Longitude: 163.0300°W
 Latitude: 64.5400°N
Exposure: SSE

Top 10 surge events between 1954 and 2004

	Starting Date	Maximum Surge (ft MLLW)	Minimum Surface Pressure (mb)	Maximum Wind	
				Speed (mph)	Direction
1	01-Oct-60	13.14	975.5	48.1	SW
2	10-Nov-74	12.74	975.7	41.6	SSE
3	26-Nov-70	10.32	998.0	41.4	SW
4	08-Nov-78	10.05	997.9	38.9	SSE
5	15-Oct-04	10.02	979.9	39.6	ESE
6	14-Nov-66	9.96	998.0	46.5	SSE
7	25-Oct-96	9.33	1004.6	34.2	S
8	25-Aug-75	8.74	997.2	37.8	S
9	12-Nov-65	8.15	971.6	42.7	S
10	06-Nov-85	8.12	993.4	39.4	SE

Frequency of Occurrence

Return Period (years)	5	10	15	20	25	50	100
Surge Level (ft MLLW)	6.90	8.91	9.82	10.28	10.71	12.97	15.53
Std. Deviation (ft)	0.75	0.85	0.69	0.98	1.21	2.69	3.38

Shaktoolik
Location:
Longitude: 161.1500°W
Latitude: 64.3300°N
Exposure: SW

Top 10 surge events between 1954 and 2004

	Starting Date	Maximum Surge (ft MSL)	Minimum Surface Pressure (mb)	Maximum Wind	
				Speed (mph)	Direction
1	01-Oct-60	14.27	977.8	47.2	SW
2	10-Nov-74	12.47	981.6	40.0	SSE
3	26-Nov-70	10.73	1001.5	38.7	SW
4	14-Nov-66	10.50	1002.1	40.7	SSE
5	08-Nov-78	10.10	1001.9	37.8	SSE
6	25-Aug-75	9.19	1000.8	41.2	SSW
7	15-Oct-04	9.15	984.6	33.6	ESE
8	12-Nov-65	8.66	975.6	41.4	S
9	25-Oct-96	8.63	1008.7	25.9	S
10	18-Oct-91	7.22	1004.7	32.2	WSW

Frequency of Occurrence

Return Period (years)	5	10	15	20	25	50	100
Surge Level (ft mllw)	8.09	10.99	12.14	12.90	13.55	16.21	19.10
Std. Deviation (ft)	0.79	0.98	0.92	1.21	1.54	2.92	3.41

Unalakleet
Location:
    Longitude: 160.7900°W
    Latitude: 63.8700°N
Exposure: WSW

Top 10 surge events between 1954 and 2004

	Starting Date	Maximum Surge (ft MLLW)	Minimum Surface Pressure (mb)	Maximum Wind	
				Speed (mph)	Direction
1	01-Oct-60	16.01	980.2	47.2	SW
2	10-Nov-74	14.17	983.9	41.2	SSE
3	26-Nov-70	12.93	1003.5	37.6	E
4	14-Nov-66	12.73	1004.1	39.1	SSE
5	08-Nov-78	11.68	1003.7	38.0	SSE
6	25-Aug-75	11.32	1003.4	41.4	SSW
7	15-Oct-04	10.99	986.2	32.9	ESE
8	12-Nov-65	10.93	976.9	40.9	SSW
9	25-Oct-96	10.53	1010.6	25.5	S
10	18-Oct-91	9.28	1003.7	31.5	WSW

Frequency of Occurrence

Return Period (years)	5	10	15	20	25	50	100
Surge Level (ft MLLW)	7.71	10.76	11.88	12.80	13.42	15.49	17.32
Std. Deviation (ft)	0.79	0.98	0.98	1.31	1.38	1.94	2.13

Saint Michael
Location:
      Longitude: 162.0400°W
      Latitude: 63.4800°N
Exposure: N, E and SE

Top 10 surge events between 1954 and 2004

	Starting Date	Maximum Surge (ft MLLW)	Minimum Surface Pressure (mb)	Maximum Wind	
				Speed (mph)	Direction
1	01-Oct-60	12.98	980.9	47.2	SW
2	10-Nov-74	12.68	982.2	39.8	SSE
3	26-Nov-70	11.40	1003.3	38.0	E
4	14-Nov-66	11.17	1003.4	42.3	SSE
5	15-Oct-04	9.99	984.4	35.1	ESE
6	08-Nov-78	9.83	1002.6	37.8	S
7	25-Oct-96	9.66	1009.3	30.4	S
8	25-Aug-75	9.33	1003.5	41.4	SSW
9	12-Nov-65	9.33	975.0	44.1	S
10	16-Nov-90	8.19	997.9	26.6	SSE

Frequency of Occurrence

Return Period (years)	5	10	15	20	25	50	100
Surge Level (ft MLLW)	6.97	9.33	10.32	11.07	11.56	12.94	14.06
Std. Deviation (ft)	0.62	0.79	0.85	1.08	1.08	1.25	1.28

Agcklarok
Location:
    Longitude: 164.7700°W
    Latitude: 62.6100°N
Exposure: NW

Top 10 surge events between 1954 and 2004

	Starting Date	Maximum Surge (ft MLLW)	Minimum Surface Pressure (mb)	Maximum Wind	
				Speed (mph)	Direction
1	10-Nov-74	10.61	978.5	44.3	SSW
2	01-Oct-60	10.61	983.8	49.4	SW
3	15-Oct-04	8.81	978.5	42.3	SE
4	14-Nov-66	8.41	1001.1	50.8	SSE
5	26-Nov-70	8.25	1003.4	41.2	WSW
6	12-Nov-65	8.18	970.7	46.5	S
7	08-Nov-78	7.95	997.8	39.8	SE
8	25-Oct-96	7.59	1007.2	36.9	S
9	25-Aug-75	7.20	1004.0	42.1	SSW
10	16-Nov-90	7.07	997.4	38.0	SE

Frequency of Occurrence

Return Period (years)	5	10	15	20	25	50	100
Surge Level (ft MLLW)	5.59	7.53	8.25	8.64	9.07	10.87	12.91
Std. Deviation (ft)	0.49	0.69	0.56	0.69	0.95	1.84	2.23

Hooper Bay
Location:
> Longitude: 166.1000°W
> Latitude: 61.5300°N
Exposure: SE

Top 10 surge events between 1954 and 2004

	Starting Date	Maximum Surge (ft MLLW)	Minimum Surface Pressure (mb)	Maximum Wind	
				Speed (mph)	Direction
1	10-Nov-74	13.57	978.6	45.6	SSW
2	15-Oct-04	11.83	975.7	43.4	SW
3	12-Nov-65	11.73	968.9	47.0	SSW
4	02-Oct-92	11.70	981.6	51.2	SSE
5	06-Nov-85	11.66	994.3	43.2	ESE
6	27-Oct-95	11.60	975.0	49.7	SE
7	12-Nov-96	11.40	998.3	50.6	SE
8	08-Nov-78	11.40	997.0	45.6	SE
9	14-Nov-66	11.34	1002.0	47.9	S
10	25-Oct-96	10.78	1008.4	39.6	S

Frequency of Occurrence

Return Period (years)	5	10	15	20	25	50	100
Surge Level (ft MLLW)	9.92	11.50	11.83	12.02	12.22	13.37	14.91
Std. Deviation (ft)	0.49	0.82	0.23	0.33	0.52	1.48	2.17

Toksook Bay
Location:
    Longitude: 165.1000°W
    Latitude: 60.5300°N
Exposure: SW

Top 10 surge events between 1954 and 2004

	Starting Date	Maximum Surge (ft MLLW)	Minimum Surface Pressure (mb)	Maximum Wind	
				Speed (mph)	Direction
1	12-Nov-65	13.60	974.0	53.2	S
2	27-Oct-95	11.96	975.7	53.0	SE
3	02-Oct-92	11.83	986.7	53.9	SSE
4	10-Nov-74	11.56	984.9	44.3	S
5	12-Nov-96	10.88	999.3	53.2	SE
6	02-Nov-78	10.65	967.7	50.3	SE
7	07-Nov-79	10.61	982.7	46.8	SSW
8	08-Nov-78	10.02	1002.0	45.6	SE
9	17-Nov-93	9.47	981.6	44.1	SSE
10	19-Nov-04	9.43	972.7	51.0	ESE

Frequency of Occurrence

Return Period (years)	5	10	15	20	25	50	100
Surge Level (ft MLLW)	8.45	10.19	11.04	11.53	11.93	12.98	13.86
Std. Deviation (ft)	0.52	0.69	0.69	0.82	0.75	0.98	1.18

Mekoryuk
Location:
        Longitude: 166.1900°W
        Latitude: 60.3900°N
Exposure: NNW

Top 10 surge events between 1954 and 2004

	Starting Date	Maximum Surge (ft MLLW)	Minimum Surface Pressure (mb)	Maximum Wind	
				Speed (mph)	Direction
1	10-Nov-74	8.28	983.2	45.6	S
2	12-Nov-65	7.86	972.5	51.4	WSW
3	15-Oct-04	7.23	979.2	42.5	SW
4	06-Nov-85	6.84	994.7	44.1	E
5	27-Oct-95	6.84	971.2	50.1	SE
6	19-Nov-04	6.71	970.0	51.4	ESE
7	01-Oct-60	6.61	990.1	45.9	WSW
8	08-Nov-78	6.61	1000.3	47.2	SE
9	02-Oct-92	6.38	985.6	51.9	SSE
10	12-Nov-96	6.28	996.0	53.2	SE

Frequency of Occurrence

Return Period (years)	5	10	15	20	25	50	100
Surge Level (ft MLLW)	5.53	6.41	6.74	6.97	7.23	8.19	9.27
Std. Deviation (ft)	0.23	0.30	0.26	0.39	0.56	1.08	1.35

Kongiganak
Location:
        Longitude: 163.0500°W
        Latitude: 59.8800°N
Exposure: SE

Top 10 surge events between 1954 and 2004

	Starting Date	Maximum Surge (ft MLLW)	Minimum Surface Pressure (mb)	Maximum Wind	
				Speed (mph)	Direction
1	27-Oct-95	16.97	982.2	50.1	SE
2	12-Nov-65	15.69	981.4	46.5	S
3	07-Nov-79	15.36	988.1	39.1	SW
4	02-Oct-92	13.82	992.0	54.1	SSE
5	02-Nov-78	13.29	973.3	48.1	SE
6	12-Nov-96	12.87	1004.1	48.3	SE
7	10-Nov-74	12.61	983.2	42.9	S
8	19-Nov-04	12.31	977.0	45.6	ESE
9	08-Nov-78	11.06	1008.2	41.6	SE
10	06-Nov-85	10.74	997.2	42.9	ESE

Frequency of Occurrence

Return Period (years)	5	10	15	20	25	50	100
Surge Level (ft MLLW)	10.31	12.57	13.92	14.84	15.43	17.03	18.28
Std. Deviation (ft)	0.52	1.05	1.21	1.38	1.28	1.35	1.28

Dillingham
Location:
Longitude: 158.4600°W
Latitude: 59.0400°N
Exposure: S

Top 10 surge events between 1954 and 2004

	Starting Date	Maximum Surge (ft MLLW)	Minimum Surface Pressure (mb)	Maximum Wind	
				Speed (mph)	Direction
1	07-Nov-79	23.90	994.4	49.0	SSW
2	12-Nov-65	20.53	989.4	50.1	SSW
3	10-Nov-74	20.26	981.1	46.3	S
4	02-Nov-78	20.00	978.0	47.2	SSE
5	19-Nov-04	19.90	975.8	49.0	SE
6	27-Oct-95	18.43	983.5	58.8	SE
7	12-Nov-89	17.70	990.8	39.6	S
8	02-Oct-92	17.21	993.4	47.0	SSE
9	20-Sep-98	17.08	985.0	37.1	S
10	15-Oct-72	16.56	980.3	39.8	SE

Frequency of Occurrence

Return Period (years)	5	10	15	20	25	50	100
Surge Level (ft MLLW)	15.74	17.64	19.08	19.84	20.39	22.69	24.27
Std. Deviation (ft)	0.46	1.12	1.21	1.28	1.38	2.59	3.22

74

Cape Newenham
Location:
    Longitude: 162.1000°W
    Latitude: 58.6500°N
Exposure: S and W

Top 10 surge events between 1954 and 2004

	Starting Date	Maximum Surge (ft MLLW)	Minimum Surface Pressure (mb)	Maximum Wind	
				Speed (mph)	Direction
1	07-Nov-79	7.55	1002.5	38.0	SW
2	12-Nov-65	6.50	996.0	41.8	SSW
3	27-Oct-95	5.54	998.5	49.0	SE
4	02-Nov-78	5.02	978.0	38.5	SE
5	10-Nov-74	4.20	986.1	36.9	S
6	19-Nov-04	4.04	975.8	37.4	SE
7	02-Oct-92	3.28	992.1	32.0	SSE
8	15-Oct-72	3.22	989.2	36.9	SSE
9	12-Nov-89	3.18	995.0	32.0	S
10	01-Oct-63	3.18	985.4	35.8	WNW

Frequency of Occurrence

Return Period (years)	5	10	15	20	25	50	100
Surge Level (ft MLLW)	6.69	7.51	8.33	9.11	9.67	11.67	13.44
Std. Deviation (ft)	0.23	0.59	0.85	1.25	1.35	1.87	2.03

Appendix D: Empirical Simulation Technique

The Empirical Simulation Technique (EST) or the extended "bootstrap" approach is a statistical resampling, nearest neighbor, random-walk interpolation technique that uses historical data to develop joint probability relationships among the various measured storm parameters. There are no simplifying assumptions concerning the development of probability density functions describing historical events. Thus, the interdependence of parameters is maintained. In this manner, parameter probabilities are site specific, do not depend on fixed parametric relationships, and do not assume parameter independence. Thus, the EST is distribution free and nonparametric. The EST was first developed to model multi-parameter events such as tropical hurricanes in which storms can be described in terms of defined storm parameters such as central pressure deficit, radius to maximum winds, maximum winds, minimum distance from the eye of the storm to the location of interest, forward speed of the eye, and tidal phase during the storm event. The extra-tropical storm events (northeasters) modeled during this study are not well represented by such a parameterization and as such the one-dimensional version of has been adopted. A complete description of the EST may be found in Scheffner and Borgman (1992), Borgman et al. (1992) and Scheffner et al. (1999).

The only assumption in the EST is that future events will be statistically similar in magnitude and frequency to past events. The 1D EST begins with an analysis of historical events that have impacted the region of interest. A storm response is defined for each event in the frequency-of-occurrence analysis. In the present application, the response is the maximum water-surface elevation induced by the storm, which includes the storm surge computed via ADCIRC, the additional water level increases due to atmospheric pressure (inverted barometer), and the tides. Implementation of the 1D EST begins with the selection of a subset of storm events that is representative of the entire set of historical storms. This subset is referred to as the "training set." The training set usually includes historical events but may include historical storms with a deviation or perturbation, such as a storm with a slightly altered path. Some historical events may also be deleted from the training set if two events are nearly identical such that both would produce the same response. Because the purpose is to fill the parameter space, two similar events are redundant. The training set can be augmented with additional storms contained in the historical data set. Storm events augmenting the training set are referred to as the "statistical set" of storms. Whereas numerical models are used for generating response vectors for those events in the training set, re-

sponse vectors for the statistical set of storms are interpolated using the training set response vectors. Thus, stage-frequency relationships can be generated using the entire historical data set without need of simulating all storms in that data set. With the augmented storm data set (i.e., training and statistical storm sets), the EST produces N simulations of a T-year sequence of storm events, each with their associated input vectors and response vectors. Because there are N-repetitions of a T-year sequence of events, an error analysis of the results can be performed with respect to median, worst, least, standard deviations, etc. The following describes the procedures by which the input and response data are used to produce multiple simulations of multiple years of events.

Two criteria are required of the T-year sequence of events. The first criterion is that the individual events must be similar in behavior and magnitude to historical events, i.e., the interrelationships among the input and response vectors must be realistic. The second criterion is that the frequency of storm events being modeled by the EST is identical to the historical frequency of storm events. The following sections describe how these criteria are preserved.

Storm-Event Consistency

The first major assumption in the EST is that future events will be similar to past events. This criterion is maintained by ensuring that the input vectors for simulated events have similar joint probabilities as those in the training set. For example, a hurricane with a large central pressure deficit and low maximum winds is not a realistic event; the two parameters are not independent although their precise dependency is unknown. The simulation of realistic events is accounted for in the nearest neighbor interpolation, bootstrap, and resampling technique developed by Borgman et al. (1992). The basic technique can be described in two dimensions as follows. Let X_1, X_2, X_3, ..., X_n be n independent, identically distributed random vectors (i.e., storm events), each having two components [$X_i = \{\underline{x}_i(1)$, $\underline{x}_i(2)\}$; $i = 1,n$] (i.e., storm parameters such as pressure deficit and wind speeds). Each event X_i has a probability p_i as $1/n$; therefore, a cumulative probability relationship can be developed in which each storm event is assigned a segment of the total probability ranging from 0 to 1. If each event has an equal probability, then each event is assigned a segment s_j. Therefore, each event occupies a fixed portion of the 0 to 1 probability space ac-

cording to the total number of events in the training set, which can be defined mathematically as:

$$\left[0 < s_1 \leq \frac{1}{n} \right]$$

.

$$\left[\frac{1}{n} < s_2 \leq \frac{2}{n} \right]$$

.

$$\left[\frac{2}{n} < s_3 \leq \frac{3}{n} \right] \qquad \text{(D-1)}$$

.

.

.

$$\left[\frac{n-1}{n} < s_n \leq 1 \right]$$

A random number from 0 to 1 is selected and used to identify a storm event from the total storm population. The procedure is equivalent to drawing and replacing random samples from the full storm-event population.

The EST is not simply a resampling of historical events technique, but rather an approach intended to simulate the vector distribution contained in the training set population. The EST approach is to select a sample storm based on a random number chosen from the range of 0 to 1 and then perform a random walk from the selected event X_i (with x_1 and x_2) vectors to the nearest neighbor vectors. The walk is based on independent uniform random numbers ranging from -1 to 1 and has the effect of simulating responses that are not identical to the historical events themselves, but are similar to those events that have historically occurred.

Storm-Event Frequency

The second criterion to be satisfied is that the total number of storm events selected in the T-years must be statistically representative of the number of historical events that have occurred at the area of interest. Given the mean frequency of storm events for a particular region, a Poisson distribution is used to determine the average number of expected events in a given year. For example, the Poisson distribution can be written in the following form:

$$Pr(s;\lambda) = \frac{\lambda^s e^{-\lambda}}{s!} \qquad\qquad \text{(D-2)}$$

for $s = 0,1,2,3,....$ The probability $Pr(s;\lambda)$ defines the probability of having s events per year where λ is a measure of the historically based number of events occurring per year.

A 10,000-element array is initialized to the above Poisson distribution. The probability corresponding to $s = 0$ storms per year, or no storms occurring in a particular year, is 0.8056; thus, if a random number selection is less than or equal to 0.8056 on an interval of 0 to 1, then no hurricanes would occur during that simulation year. If the random number falls between 0.8056 and 0.9798 (where the latter value, 0.9798, is found by adding $Pr[s = 0]$ and $Pr[s = 1]$ together, or 0.8056 + 0.1742), one event is selected. Two events are simulated if a random number is selected within the range of 0.9798 and 0.9986 (where 0.9986 = $Pr[s = 0]$ + $Pr[s = 1]$ + $Pr[s = 2]$ = 0.8056 + 0.1742 + 0.0188), etc. When one or more storms are indicated for a given year, they are randomly selected using the nearest neighbor interpolation technique described above.

Output from the EST program is N repetitions of T-years of simulated storm-event responses. It is from these responses that frequency-of-occurrence relationships are computed. The computational procedure followed is based on the generation of a probability distribution function corresponding to each of the T-year sequence of simulated data.

Recurrence Relationships

Estimates of frequency-of-occurrence relationships begin with calculating a cumulative distribution function (cdf) for the response vector

of interest, the maximum water-surface elevation. Let X_1, X_2, X_3, ..., X_n be n identically distributed random-response variables with a cumulative cdf

$$F_X \ (x) = \ Pr[X \le x] \tag{D-3}$$

where $Pr[\ ]$ represents the probability that the random variable X is less than or equal to some value x and $F_X(x)$ is the cumulative probability distribution function ranging from 0 to 1. The problem is to estimate the value of F_X without introducing some parametric relationship for computing the probability. The following procedure is adopted because it makes use of the probability laws defined by the data and does not incorporate any prior assumptions concerning the probability relationship.

Assume a set of n observations of data. The n values of x are first ranked in order of increasing size such that $x_{(1)} \le x_{(2)} \le x_{(3)} \le \ldots \le x_{(n)}$, where the parentheses surrounding the subscript indicate that the data have been rank ordered. The value $x_{(1)}$ is the smallest in the series, and $x_{(n)}$ represents the largest. Let r denote the rank of the value $x_{(r)}$ such that rank 1 is the smallest and rank $r = n$ is the largest.

An empirical estimate of $F_X \ (x_{(r)})$, denoted by $\hat{F}_X \ (x_{(r)})$, is given by Gumbel (1954) (see also Borgman and Scheffner (1991) or Scheffner and Borgman (1992)).

$$\hat{F}_x(\ x_{(r)})= \frac{r}{(n+1)} \tag{D-4}$$

for $\{x_{(r)}, \ r = 1, 2, 3,...., n\}$. This form of estimate allows for future values of x to be less than the smallest observation $x_{(1)}$ with probability of $1/(n+1)$ and to be larger than the largest value $x_{(n)}$ with probability $n/(n+1)$. In the implementation of the EST, tail functions are used to define the cdf for events larger than the largest or smaller than the smallest observed event so that the cdf contains no discontinuity (Borgman and Scheffner 1991).

The estimated cdf as defined by Equation D-5 is used to develop stage-frequency relationships in the following manner. Consider that the cdf for some storm response corresponding to an n-year return period event can be determined from:

$$F(x) = 1 - \frac{1}{n} \tag{D-5}$$

where $F(x)$ is the simulated cdf of the n-year impact. Frequency-of-occurrence relationships are obtained by linearly interpolating a stage from Equation D-4 corresponding to the cfd associated with the return period specified in Equation D-5.

Because multiple simulations are made, each yielding its own stage-frequency curve relationship, the average stage is computed for each return period year. Furthermore, for each return period, the standard deviation, defined as:

$$\sigma = \sqrt{\left[(1/N) \sum_{n=1}^{n=N} (x_n - \bar{x}) \right]} \qquad \text{(D-6)}$$

(where x bar is the mean value), is computed to define an error band of $\pm$ one standard deviation corresponding to the mean value for that particular return period year.

Appendix E: Comparison of Return Period Estimates

Table E1. Return period estimates from EST

Station	Return Period, years				
	5	10	25	50	100
Kivalina	3.67	4.58	5.96	6.91	7.77
Red Dog	3.76	4.68	6.13	7.04	7.77
Kotzebue	4.06	5.05	6.85	8.59	10.56
Shishmaref	3.50	4.38	5.33	5.82	6.19
Wales	3.63	4.48	5.14	5.53	5.96
Nome	5.79	7.07	8.68	9.66	10.51
Golovin	6.90	8.91	10.71	12.97	15.53
Shaktoolik	5.77	8.69	11.25	13.91	16.80
Unalakleet	7.71	10.76	13.42	15.49	17.32
Saint Michael	6.97	9.33	11.56	12.94	14.06
Agcklarok	5.59	7.53	9.07	10.87	12.91
Hooper Bay	9.92	11.50	12.22	13.37	14.91
Toksook Bay	8.45	10.19	11.93	12.98	13.86
Mekoryuk	5.53	6.41	7.23	8.19	9.27
Kongiganak	10.31	12.57	15.43	17.03	18.28
Dillingham	15.74	17.64	20.39	22.69	24.27
Cape Newenham	6.69	7.51	9.67	11.67	13.44

Table E2. Return period estimates from Gumbel distribution

Station	Return period, years				
	5	10	25	50	100
Kivalina	4.75	5.31	5.83	6.13	6.39
Red Dog	4.78	5.34	5.90	6.19	6.45
Kotzebue	5.41	6.20	6.89	7.31	7.67
Shishmaref	4.12	4.61	5.10	5.40	5.63
Wales	4.15	4.61	5.04	5.27	5.46
Nome	6.97	7.79	8.51	8.97	9.33
Golovin	8.71	9.86	10.91	11.53	12.05
Shaktoolik	8.33	9.68	10.96	11.68	12.30
Unalakleet	10.24	11.58	12.80	13.52	14.14
Saint Michael	8.81	9.92	10.97	11.56	12.09
Agcklarok	7.10	8.05	8.90	9.43	9.86
Hooper Bay	10.68	11.50	12.25	12.68	13.04
Toksook Bay	9.69	10.71	11.66	12.22	12.71
Mekoryuk	6.22	6.74	7.27	7.56	7.79
Kongiganak	12.18	13.36	14.48	15.13	15.66
Dillingham	17.90	19.08	20.20	20.85	21.41
Cape Newenham	7.70	8.42	9.11	9.47	9.80

Table E3. Return period estimates from Weibull distribution

Station	Return period, years				
	5	10	25	50	100
Kivalina	4.45	5.24	6.13	6.72	7.27
Red Dog	4.49	5.40	6.45	7.18	7.83
Kotzebue	4.92	6.03	7.38	8.26	9.12
Shishmaref	3.89	4.94	6.22	7.10	7.99
Wales	4.02	4.78	5.66	6.25	6.81
Nome	6.61	7.86	9.27	10.19	11.07
Golovin	8.05	10.09	12.55	14.25	15.89
Shaktoolik	7.32	9.48	12.11	13.98	15.75
Unalakleet	9.22	11.42	14.11	16.04	17.85
Saint Michael	8.02	10.12	12.75	14.65	16.52
Agcklarok	6.54	8.15	10.05	11.40	12.64
Hooper Bay	10.52	11.96	13.57	14.65	15.67
Toksook Bay	9.47	12.02	15.27	17.60	19.90
Mekoryuk	5.99	7.00	8.25	9.07	9.89
Kongiganak	11.36	13.23	15.43	16.94	18.38
Dillingham	16.98	18.69	20.72	22.13	23.45
Cape Newenham	7.11	8.33	9.87	11.02	12.13

Table E4. Return period estimates from log-linear fit of ranked data

Station	Return period, years				
	5	10	25	50	100
Kivalina	4.22	5.11	6.29	7.21	8.09
Red Dog	4.26	5.14	6.36	7.27	8.16
Kotzebue	4.69	5.87	7.44	8.62	9.81
Shishmaref	3.89	4.64	5.66	6.42	7.17
Wales	4.05	4.74	5.63	6.32	7.01
Nome	6.51	7.66	9.20	10.38	11.56
Golovin	7.76	9.63	12.09	13.96	15.83
Shaktoolik	7.15	9.45	12.50	14.80	17.09
Unalakleet	9.15	11.38	14.37	16.63	18.90
Saint Michael	8.25	10.02	12.35	14.12	15.90
Agcklarok	6.84	8.21	10.08	11.50	12.87
Hooper Bay	10.25	11.34	12.78	13.86	14.94
Toksook Bay	9.69	11.43	13.70	15.44	17.14
Mekoryuk	6.38	7.73	9.50	10.84	2.15
Kongiganak	11.56	13.43	15.92	17.82	19.72
Dillingham	17.70	20.30	23.71	26.30	28.89
Cape Newenham	7.41	8.62	10.26	11.51	12.76
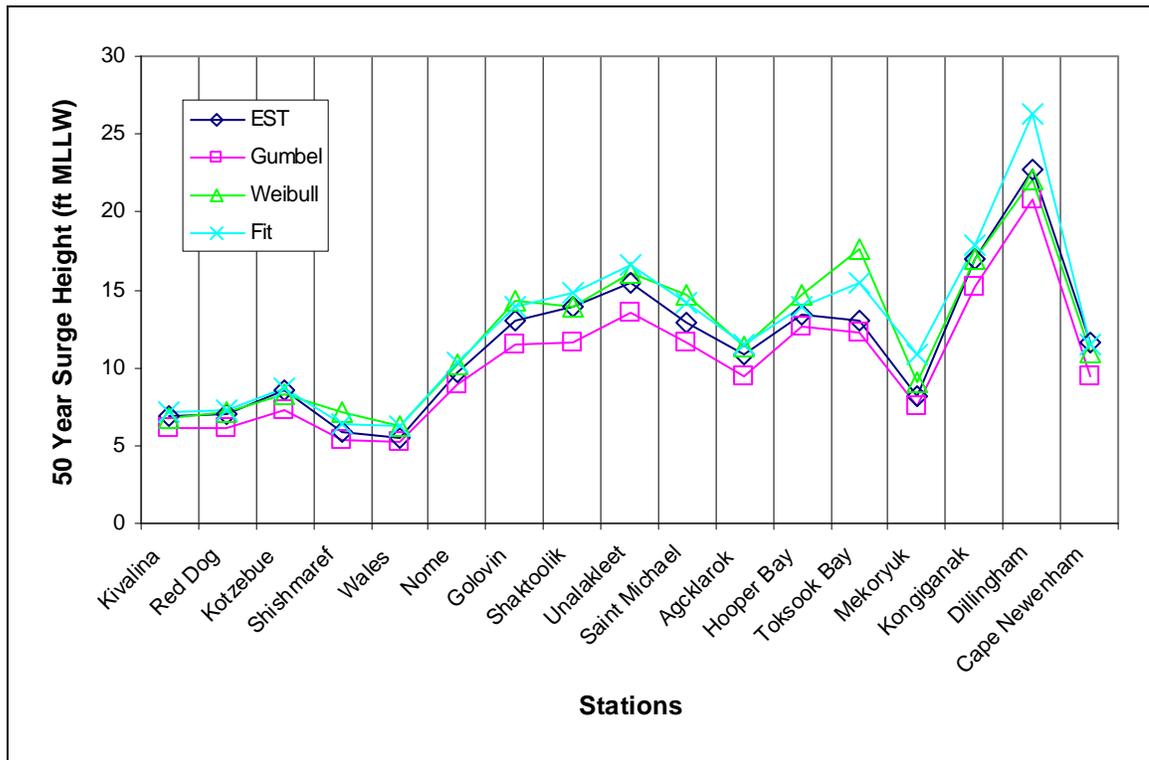
Figure E1. Estimated 50-year surge level, in feet above mllw, using 4 methods.